

Chapter 2

Laser Beam Machining

Shoujin Sun and Milan Brandt

Abstract The cost of cutting hard-to-machine materials by conventional mechanical machining processes is high due to the low material removal rate and short tool life, and some materials are not possible to be cut by the conventional machining process at all. Laser beam machining is the machining processes involving a laser beam as a heat source. It is a thermal process used to remove materials without mechanical engagement with workpiece material where the workpiece is heated to melting or boiling point and removed by melt ejection, vaporization, or ablation mechanisms. In contrast with a conventional machine tool, the laser radiation does not experience wear, and material removal is not dependent on its hardness but on the optical properties of the laser and the optical and thermophysical properties of the material. This chapter summarizes the up-to-date progress of laser beam machining. It presents the basics and characteristics of industrial lasers and the state-of-the-art developments in laser beam machining.

Symbols

$A_{r,Fe}$	The relative atomic mass of iron (55.8 g/mole)
B	Constant
b	Depth of focus
C_p	Heat capacity of solid metal
c_v	Volumetric specific heat of the melt
c_w	Specific heat of workpiece
D_{eff}	Diffusion coefficient of oxygen in liquid iron
d	Thickness of workpiece
E_{crit}^f	Critical energy density for the cutting fiber

S. Sun (✉) · M. Brandt
School of Aerospace, Mechanical and Manufacturing Engineering,
RMIT University, Bundoora, VIC 3083, Australia
e-mail: shoujin.sun@rmit.edu.au

M. Brandt
e-mail: milan.brandt@rmit.edu.au

E_{crit}^m	Critical energy density for the cutting matrix
F	Constant ($0 < F \leq 1$)
f_L	Focal length of focus optics
g	Gravitational acceleration
H	Height of nozzle from the workpiece,
ΔH	Reaction heat
I	Laser beam intensity
I_0	The maximum beam intensity at $r = 0$ (W/cm^2)
K_m	Thermal conductivity of the melt
K_0	Bessel function of the second kind and zero order
k	Thermal diffusivity of workpiece material
L_M	Latent heat of fusion
l	Distance from the stagnation point
m_{melted}	Rate of mass gain in melt layer
m_{ejected}	Rate of mass loss in melt layer
P	Incident laser power
P_a	Absorbed laser energy
P_r	Power provided by the exothermal reaction in reactive laser cutting
P_{loss}	Energy loss including these to heat the solid controlled volume to the melting temperature, latent heat of melting, and heat the liquid controlled volume to cut temperature
P_v	Energy spent for vaporization, which is negligible for melting and blow process
P_0	Stagnation pressure
P_g	Average cutting gas pressure in the cut kerf
$\partial P / \partial z$	Pressure gradient through the workpiece thickness
p_a	Ambient pressure acting on the bottom of the melt film
r	Radius of the beam (cm)
r_L	Radius of laser spot on workpiece
s	Melt layer thickness
s_{ACC}	The minimum thickness of melt if melt at the bottom of cut front by acceleration of the molten material
s_{HC}	The maximum thickness of melt film without evaporation
T_0	Room temperature
T_M	Melting point of workpiece
T_E	Boiling point of workpiece
t_{on}	Pulse duration
t_{off}	Duration of laser power off in a pulse
V	Cutting speed
V_M	Velocity of cut front
v_g	Velocity of the assist gas jet
v_m	Velocity of melt flow
\bar{v}_m	Average velocity of melt flow
We	Weber number

w	The beam radius at which $I = I_0 e^{-2}$ (86 % of the total energy is within the beam radius w)
w_0	The collimated beam radius
w_f	Radius of focused laser beam
w_k	Kerf width
z_R	Rayleigh length distance
α	Angle of inclination of the cut front
α_w	Thermal expansion coefficient workpiece
$\hat{\alpha}$	Absorptivity of laser light
β	Cut front angles at the vertical planes
β_B	Cut front angle at the bottom
η	Percentage of melt film that is oxidized
λ	Wavelength of the laser beam
μ_g	Dynamic viscosity of the assist gas
μ_m	Viscosity of melt
θ	Angle of incidence
ρ_g	Density of the assist gas
ρ_m	Density of melt
ρ_w	Density of workpiece
σ	Surface tension of melt

2.1 Brief Introduction of Laser Beam

2.1.1 Features of Laser Beam

Laser, **L**ight **A**mplification by **S**timulated **E**mission of **R**adiation, is a high-energy beam of electromagnetic radiation. The light, photon, travels as a wave through space, but behaves as a particle of energy when it encounters matter [1]. The laser differs from other incoherent light because it is:

- monochromatic
- coherent
- directional or collimated
- bright

1. Monochromaticity

Although it is never composed of only a single wavelength in laser cavity, laser beam can be considered to be monochromatic because the oscillating laser consists of very closely spaced, discrete, and narrow spectral lines (laser modes or cavity

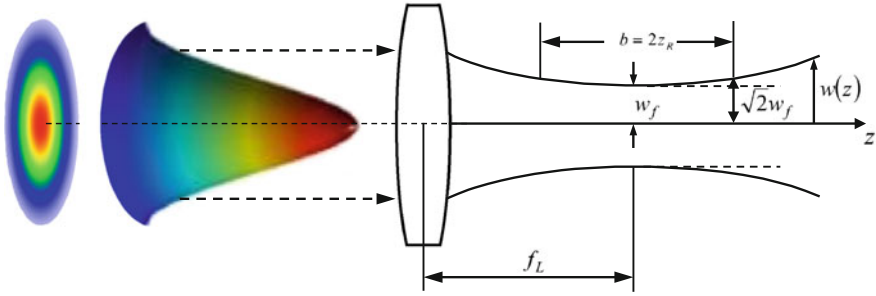


Fig. 2.1 Power distribution and focusing of TEM₀₀ Gaussian-mode laser beam

modes) compared with conventional light source whose emission covers frequency bandwidth in the order of gigahertz.

For better monochromaticity, single mode can be achieved by forcing laser to oscillate on a single transverse (usually, the fundamental TEM₀₀ Gaussian mode as shown in Fig. 2.1) and longitudinal mode.

The intensity distribution in the Gaussian beam is expressed as

$$I(r) = I_0 \exp\left(-\frac{2r^2}{w^2}\right) \quad (2.1)$$

2. Coherence

The laser beam is coherent because of the fixed-phase relationship between two waves at the wave front over time (spatial coherence) or between two points of the same wave (temporal coherence).

3. Directionality or collimation

Laser beam is directional or collimated due to its small divergence angle (Θ ranging from 0.2 to 10 milliradians except for semiconductor laser). The directionality of laser beam enables it to be focused to a very small spot over a long distance. The divergence angle (Θ) for TEM₀₀ beam is given as

$$\Theta \approx \frac{\lambda}{\pi \cdot w_0} \quad (2.2)$$

The beam quality is characterized by M^2 or the beam parameter product BPP (mm \times mrad), given by

$$M^2 = \frac{\pi}{\lambda} w_0 \cdot \Theta \quad (2.3)$$

$$\text{BPP} = w_0 \cdot \Theta \quad (2.4)$$

Table 2.1 Characteristics of common industrial lasers for material processing [6, 153, 154]

	CO ₂	Excimer	Nd:YAG	High-power diode	Fiber laser
Wavelength (μm)	10.6	0.125–0.351	1.06	0.65–0.94	1.07
BPP (mm × mrad)	12		12 ^a , 25–45 ^b	100–1,000	0.3–4
Overall efficiency (%)	5–10	1–4	1–3	30–50	10–30
Output power in CW mode	Up to 20 kW	300 W	Up to 16 kW	Up to 4 kW	Up to 10 kW
Focused power density (W/cm ²)	10 ^{6–8}		10 ^{5–7a} , 10 ^{6–9b}	10 ^{3–5}	
Pulse duration (sec)	10 ^{–4}	10 ^{–9}	10 ^{–8} –10 ^{–3}	10 ^{–12}	10 ^{–13}
Fiber coupling	No	Yes	Yes	Yes	Yes

^a Pumped by flash lamp^b Pumped by diode

4. Brightness

Brightness measures the capability of a laser oscillator to emit a high optical power per unit area per unit solid angle, which is related to the directionality of the laser beam. Smaller divergence angle results in higher brightness. Laser beam machining process requires a laser beam with high brightness (BPP is generally smaller than 20 at power level of kW).

Lasers are normally classified based on the physical states of the laser-active (pumping) medium as gas lasers (CO₂ and excimer), solid state lasers (Nd:YAG), semiconductor lasers (diode), liquid lasers, and fiber lasers (Yb:YAG). Characteristics of the common industrial lasers are listed in Table 2.1.

The excimer laser may be characterized by its intense UV-wavelength pulses which remove material by unique photochemical ablation process [2]. The excimer laser is normally used to process organic materials.

Despite their high efficiency, diode lasers have low beam quality with high beam parameter product, which limits these lasers being applied in cutting, drilling, marking on metallic materials, and micromachining [3]. However, high-power diode lasers are well suitable for preheating workpiece for laser-assisted machining for example.

The most important characteristics of high-power laser for cutting are [4] as follows:

1. The beam must as close as possible to the fundamental TEM₀₀ radial mode;
2. Both output power and its radial distribution must be temporarily constant in the continuous wave mode.

2.1.2 Manipulation of Laser Beam

Laser beam can be manipulated through optics such as follows:

Focusing: Laser beam can be focused by curved mirrors or lenses to reduce its spot size. The radius of focused Gaussian-mode laser beam (w_f) is the smallest laser beam radius at the plane $z = 0$ as shown in Fig. 2.1:

$$w_f = \frac{f_L \cdot \lambda}{\pi \cdot w_0} M^2 = f_L \cdot \Theta. \quad (2.5)$$

The depth of focus (b) is twice the Rayleigh length distance z_R , which is defined as the distance from the focus at which the cross-sectional area of the laser beam has doubled (or the beam radius increases by a factor of $\sqrt{2}$).

$$b = 2z_R = \frac{2\pi \cdot w_f^2}{\lambda \cdot M^2} \quad (2.6)$$

It indicates in Eqs. (2.5) and (2.6) that both the focused radius and depth of focus of a laser beam with Gaussian mode increase with the focal length of focusing optics.

Shaping (spatial shaping): The commonly used laser beam for cutting purpose is the Gaussian beam (TEM_{00}), but it can be shaped into other profiles such as top-hat and rectangular beams, which have a complex power distributions rather than a Gaussian distribution as shown in Fig. 2.1.

Pulsing (temporal shaping): The laser beam can be emitted temporally in either the continuous wave (CW) or pulse modes. The power of laser beam is constant in the continuous wave mode, but intermittent in the pulse mode. The pulse laser beam is characterized with peak power, pulse duration (length or width), and pulse frequency (repetition frequency). The advantage of the pulsed laser is its increasing peak power with shorter pulse duration without an increase in the average output (except in the case of gated pulsing). From the processing point of view, the depth of heat conduction (heat-affected zone) into workpiece is lower compared with that of CW laser [5]. Laser pulse shape can be manipulated to generate a rectangular, smooth, and triangular pulses.

Pulsed laser beam can be classified into three categories [6]:

1. Gated pulsing: peak power is about the same with nominal output power in CW mode
2. Superpulsing: The peak power is higher than the average output power depending on the pulse frequency and duty cycle.
3. Hyperpulsing: High peak power pulses are superimposed on the CW output power.

The pulsing is achieved by normal pulsing, Q switching (generation of ns pulses), and mode locking (for the generation of pulses with pulse widths below 100 picoseconds down to a few femtoseconds).

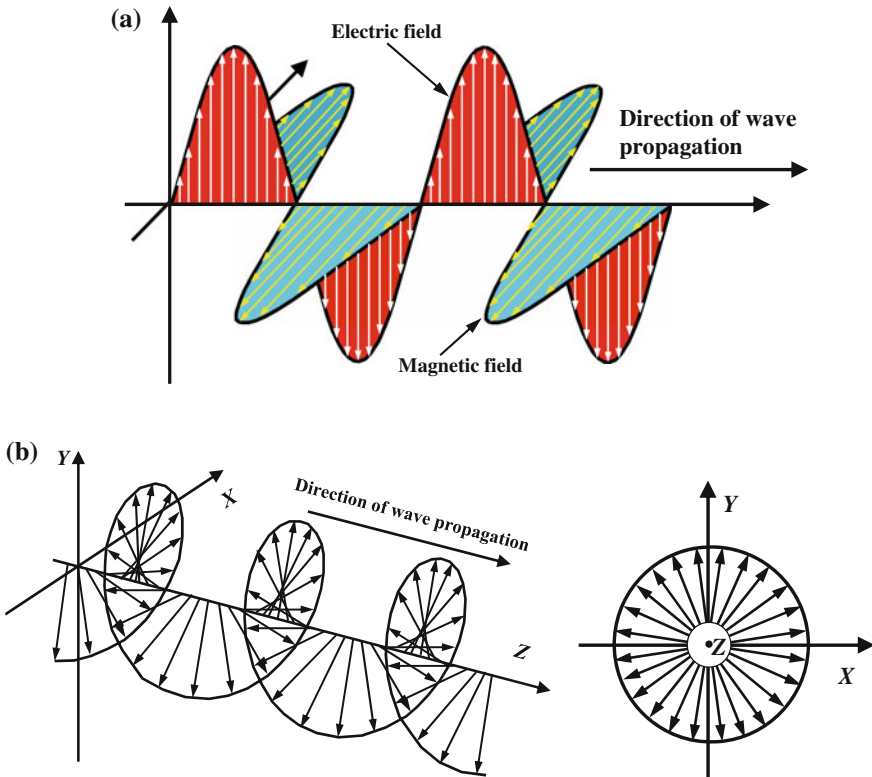


Fig. 2.2 Electric field vector in (a) linearly and (b) circularly polarized beams

Polarization: laser beam emitted from the laser cavity can be linearly polarized, that is, the vectors of the oscillating electric and magnetic field of the traveling photons are perpendicular to each other and to the propagating direction; the electric field vector oscillates only in one plane (as shown in Fig. 2.2a).

In order to eliminate the effect of orientation of electric field vector, the laser beam can be depolarized through optical device (depolarizer) as a circularly polarized beam in which the direction of the electric field vector rotates about its propagation direction while it retains constant magnitude. The tip of the electric field vector, at a given point in space, describes a circle as time progresses (as shown in Fig. 2.2b).

Splitting: A laser beam can be split into multiple beams with various power ratios between beams by using an optical device (beam splitter) through the methods of reflection, interference, or polarization.

Spinning: A focused beam is shifted laterally by rotating mirror or window to cover wider area.

2.2 Characteristics of Laser: Material Interaction

2.2.1 Photochemical (Photolytic) Process

When a material (normally an organic material) is irradiated by a short-wavelength (in UV range, such as excimer laser) and short-pulse-length (shorter than the thermal relaxation time in microseconds) laser beam, the molecular bonds in a very thin layer of the material surface can be broken by the higher energy of shorter-wavelength photon with minimum thermal effect, and this is also called “cold-cutting.” The photon energies between 3.60 and 4.29 eV within the wavelength between 344 and 288 nm are high enough to break C–C and C–H covalent bonds (with average binding energies of 347 kJ/mol and 414 kJ/mol, respectively) [7].

2.2.2 Photothermal (Pyrolytic) Process

When a laser beam irradiates the workpiece surface, part of the laser beam energy is absorbed by the workpiece surface due to the interaction between the electromagnetic radiation and electrons of the workpiece materials. The remaining is lost due to the reflection by the workpiece surface.

The absorption rate, or absorptivity, characterizes the percentage of incident laser power that is absorbed by a solid workpiece material. It is affected by the wavelength of laser beam (as shown in Fig. 2.3), polarization of beam, characteristics of workpiece material (chemical composition, surface condition, and temperature), and beam incident angle.

The laser beam absorption increases with surface roughness only when it exceeds a roughness threshold, which is dependent on the type of workpiece

Fig. 2.3 Absorption and reflection rates as a function of beam wavelength for various metals (drawn in reference to [146])

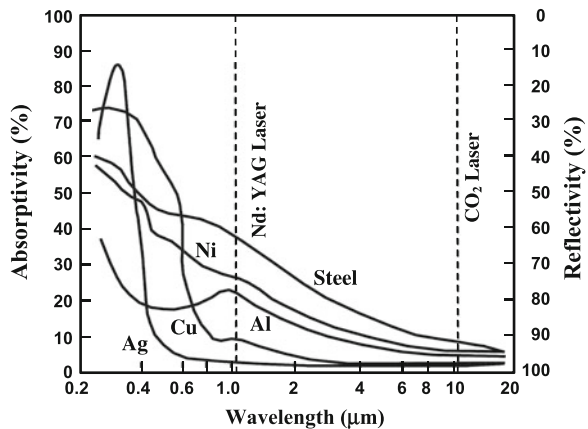
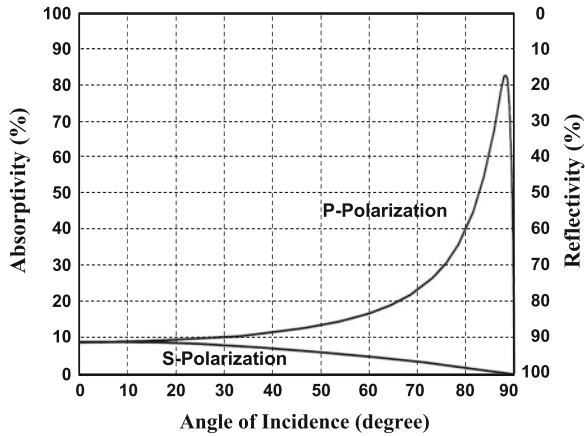


Fig. 2.4 Variation of reflectivity and absorptivity of iron to the linearly polarized CO₂ laser beam with angel of incidence (drawn in reference to [147])

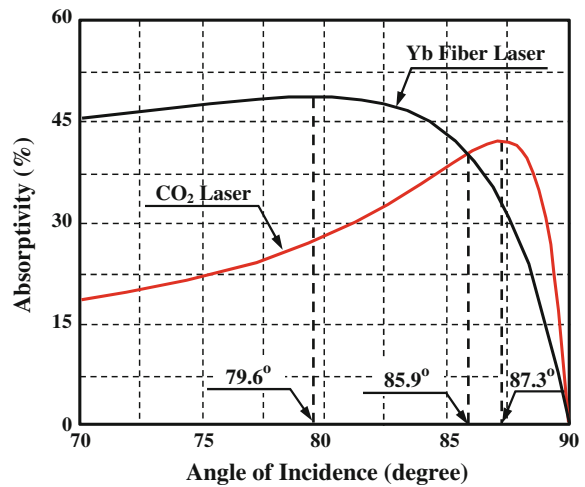


materials, and the relationship between absorption and surface roughness is affected by the beam incident angle [8].

The beam incident angle has a strong effect on the absorption of linearly polarized beam, which is determined by Fresnel absorption [6, 9]. Generally, the refecton of s-polarized beam (the electric field vector is normal to the plane of incidence) is higher than that of the p-polarized beam (the electric field vector is in the plane of incidence) as shown in Fig. 2.4. Brewster's angle at which the absorptivity of the incident beam reaches maximum is very high and near 90°.

The dependence of absorptivity on angle of incidence for unpolarized laser beam is strongly affected by the beam wavelength as shown in Fig. 2.5. The Brewster's angle is 79.6° and 87.3° for fiber laser with wavelength of 1.07 μm and CO₂ laser with wavelength of 10.6 μm, respectively. The absorptivity of molten

Fig. 2.5 Effect of angle of incidence on absorptivity of molten iron for unpolarized laser beams with different wavelengths (reprinted from Mahrle and Beyer [31] with permission. Copyright © IOP Publishing Ltd)



iron for fiber laser radiation is better than that for CO₂ laser radiation only when the angle of incidence is smaller than 85.9°.

Surface directionality due to the mechanical surface finish is also found to affect the absorption of polarized light [10].

The absorbed laser energy is converted to the thermal energy to cause a significant temperature rise on the surface of the workpiece, which can

1. induce thermal stress in the heat-affected zone if the surface temperature is lower than the melting point;
2. melt the surface of material when the surface temperature is higher than the melting point, but lower than the boiling point;
3. vaporize the surface of material when the surface temperature is higher than the boiling point.

Vaporization occurs on the material surface when the surface temperature reaches its boiling point with high laser intensity ($>10^8$ W/cm²), which is usually achieved with pulsed laser (superpulsing or hyperpulsing). Recoil pressure is generated on the melt surface due to the vapor evolution, which can push the melt layer from the molten zone when the tangential recoil pressure exceeds the surface tension [11]. Because the material surface is partially melted and vaporized, the material removal process without assist gas comprises both melt expulsion due to the recoil pressure and vaporization [12].

A plasma plume may be formed at or near to the surface of the materials as the result of interaction between laser beam and vapor. This plasma plume would absorb most of the incident beam energy and lead to decoupling of the incident beam from the workpiece surface [13], thereby lowering the process efficiency [14]. The proportion of incident laser power absorbed by the plasma is lower with a shorter wavelength of laser. Hence, the material removal rate is higher for shorter-wavelength laser radiation during ablation [2].

2.3 Laser Beam Machining

2.3.1 Integration of Laser System for Cutting Operation

In order to process workpiece, the laser beam has to be delivered and integrated with a motion control system. This system comprises the following:

1. Beam delivery system

Due to its long wavelength, CO₂ laser cannot be transmitted through optical fibers. Therefore, it can only be delivered to the workpiece by a series of metallic mirrors, whereas the other industrial lasers due to their shorter wavelength can be delivered by optical fiber, which offers higher degree of freedom and flexibility in a manufacturing environment.

2. Cutting head

It consists of beam delivery optics, focusing lens and gas delivery nozzle, which is usually assembled coaxially with laser beam. Two jets of gas are possibly delivered by the nozzle: one to the laser spot to remove the melted metal and the other to the surrounding of laser beam to prevent oxidation as shielding gas. The head is positioned to ensure that the laser beam is incident perpendicular to the surface of the workpiece. The gap between the nozzle and surface of workpiece must be maintained constant and at a specified stand-off distance.

3. Workpiece positioning

The relative motion between laser beam and workpiece can be achieved by either moving the workpiece only, or moving cutting head only or moving both cutting head and workpiece (hybrid system).

Flying optics: the relative movement of the laser spot can be achieved by moving only mirrors and the focusing lens while the workpiece remains stationary for remote cutting without gas jet, which allows high positioning and processing speeds with high precision and change in spot size.

2.3.2 Laser Beam Machining Processes

Some laser beam machining processes are summarized in Table 2.2. In photo-thermal processes, material can be machined by the following:

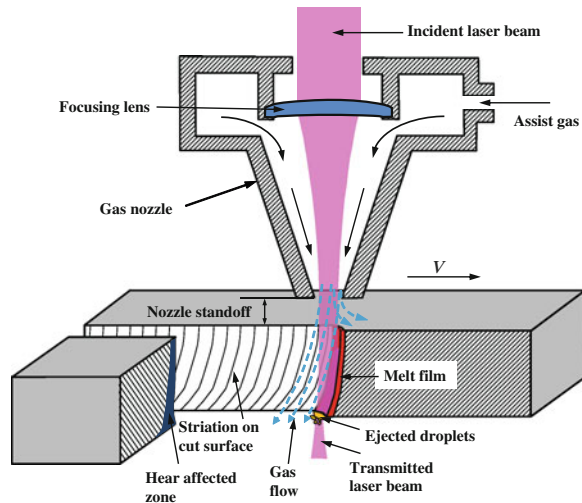
- (1) Controlled fracture process: brittle materials (ceramics) are separated by thermally induced stress cracking, which requires very low energy. Cutting speed or thickness of workpiece can be increased by employing dual-beam CO₂ laser [15] or two lasers [16]. It can be done in air or with water jet quenching after laser radiation [17]. The cutting speed with water assistance is reported to be 500 % faster than that in dry machining [18]. However, crack initiation and propagation at corners and curves during profile cutting is difficult to control and leads to cut deviation [19].
- (2) Melting and blow process: The surface of workpiece is heated and melted by laser beam (and exothermic heat if reactive gas is used) and forms an erosion/cutting front (a layer of molten material). The erosion/cut front that extends through the thickness of the workpiece is subsequently blown away by a pressurized gas jet through a coaxial nozzle (positioned coaxially with the laser beam) or off-axis nozzle as shown in Fig. 2.6. It is classified as laser fusion cutting in the case of inert gas and reactive laser cutting when a chemically reactive gas is used.

The CO₂ and Nd:YAG lasers are the two industrial lasers used for decades for removing material by melting and evaporation. Despite its lower average power

Table 2.2 Summary of laser beam machining processes [155]

	Photo-thermal processes				Photo-chemical process
	Controlled fracture	Melting and blow		Vaporization	
		Fusion	Reactive		
Mechanism	Material is broken as the result of thermally induced stress	Material is melted as a result of laser radiation, and the melt is blown by pressurized gas jet	Material is melted as a result of laser radiation and exothermic energy, the melt is blown by pressurized gas jet	Material is vaporized as a result of high intensity of laser beam radiation	Material is separated as the result of broken covalent bonds by photon energy of UV light
Relative laser energy required	1	20	10	40	100
Gas type	Inert gas	Inert gas	Chemically reactive gas	Inert gas or no gas	Inert gas
Workpiece materials	Ceramics	Metals, polymers, ceramics, glasses, composites	Metals, polymers	Metals, ceramics, polymers	Organic materials

Fig. 2.6 Illustration of laser beam cutting process (drawn in reference to [148])



compared with CO₂ laser (for cutting thick material >10 mm), the Nd:YAG laser offers relatively high peak power in the pulse mode due to its shorter pulse duration (as shown in Table 2.1) and better focusing properties and therefore the better cut quality in terms of kerf width, heat-affected zone (HAZ), and cut edge quality. Due to its smaller thermal load, Nd:YAG laser can machine brittle ceramic materials which CO₂ laser cannot machine without cracks [20]. Due to its shorter wavelength, pulsed Nd:YAG laser can be absorbed more effectively by the highly reflective metallic workpiece as shown in Fig. 2.3. Another advantage of Nd:YAG lasers is their transportability by optical fiber, which makes the cutting system more flexible and output beam non-polarized.

(3) Evaporation (sublimation cutting) process:

The material is removed by vaporization and the recoil pressure generated as vapor evolution as the surface temperature reaches the boiling point. The energy required for evaporation is estimated to be 6 times the energy required for fusion cutting [21].

This chapter is concentrated on the laser beam machining with material removed by melting and ejection because of its wide applicability to cut a large variety of materials. Some examples involving partial vaporization are also briefly discussed.

2.3.2.1 Process Analysis

The top and side views of a laser cutting process are shown in Fig. 2.7. A layer of melt at an angle of inclination (α) is produced through the thickness of workpiece as a result of heat input from laser beam in laser fusion cutting or laser power plus

Fig. 2.7 **a** Top view and **b** side view of cut front (drawn in reference to [29, 48, 61, 149]). Note the different scales in (a) and (b)

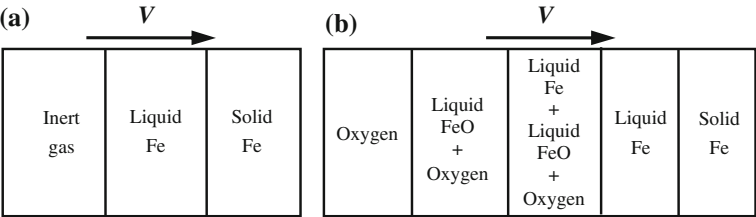
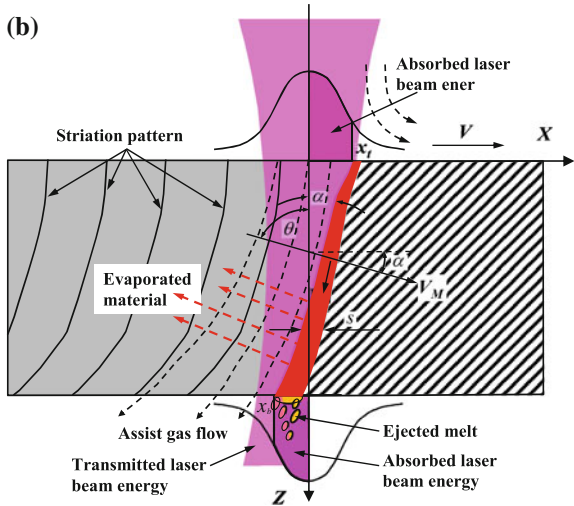
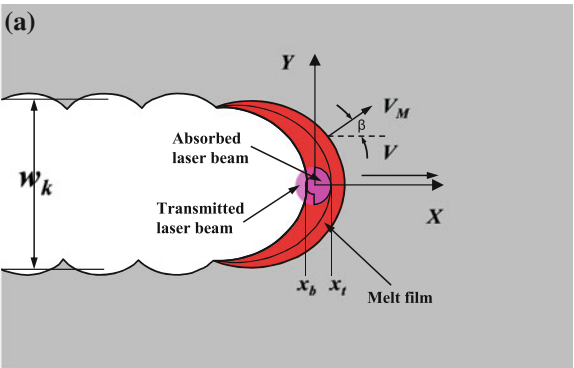


Fig. 2.8 Boundaries in the cut front for **(a)** laser fusion cutting and **(b)** oxygen-assisted laser cutting of mild steel (drawn in reference to [39])

exothermic heat in reactive laser cutting. A pressurized gas jet is used to eject the melt out of the kerf in the direction of cut front plane in order to keep the process ongoing when the laser beam is moving relative to the workpiece. Vaporization and melt expulsion by recoil pressure can contribute to the melt ejection at cutting

temperature above the boiling point as in laser fusion cutting and remote cutting process, the material lost by evaporation due to recoil pressure is predominantly in the direction perpendicular to the cut front [22].

The boundaries in the cut front are schematically shown in Fig. 2.8 for both laser fusion cutting and oxygen-assisted laser cutting of mild steel.

1. The melt front: the boundary between solid and liquid moves depending on the heat balance at the boundary [23].
2. The melt surface: the boundary between liquid and gas moves depending on the heat balance affected by laser beam absorption, melt flow, and heat conduction [23].
3. The oxidation front in reactive laser cutting: the boundary between liquid Fe and oxide layer moves dynamically at the velocity determined by diffusion of oxygen through oxide layer [24–27] or by the diffusion of iron through oxide layer [28].

The laser cutting process involves the following balances as listed in Table 2.3 for both the steady state and dynamic state. The temperature is denoted as T and thickness s of the melt fluctuate in the dynamic state.

The energy input includes the following:

1. the absorbed laser power at the cut front

Only partial laser beam is incident on the cut front (from x_b at the bottom surface to x_t at the top surface as shown in Fig. 2.7). Therefore, part of laser power is lost due to transmission through the kerf when the beam is outside the x_b . Hence, increase in the horizontal lag between the top and bottom of cut front ($x_t - x_b$) enables more laser energy to be absorbed at the cut front. The absorbed laser energy is written as [29]

$$P_a = \hat{\alpha} \int_0^{x_t} I(r, z = 0) r \pi dr + \hat{\alpha} \int_{x_b}^0 I(r, z = d) r \pi dr \quad (2.7)$$

Table 2.3 List of balances at the cut front

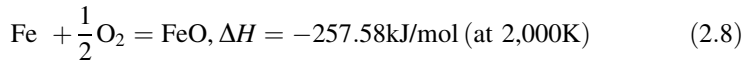
	Steady state [29]	Dynamic state [49]
Mass balance	$m_{\text{melted}} = m_{\text{ejected}}$	$m_{\text{melted}} - m_{\text{ejected}} = \rho_m \cdot d \cdot w_k \cdot \frac{ds}{dt}$
Energy balance	$P_a + P_r = P_{\text{loss}} + P_v$	$P_a + P_r - P_{\text{loss}} + P_v$ $= c_v \cdot d \cdot w_k \cdot s \cdot \frac{dT}{dt} + c_v \cdot d \cdot w_k \cdot T \cdot \frac{ds}{dt}$
Momentum balance	$F_0 + F_n + F_t = F_a + F_{\text{st}} + F_d + F_m$	

P_{loss} , the energy losses including those to heat the solid controlled volume to the melting temperature, latent heat of fusion, and heat the liquid controlled volume to cut temperature, and power loss by heat conduction to the surrounding solid workpiece. The contributions of heat loss by convection and radiation are negligible compared with conduction loss [30, 32, 39, 50], P_v , the energy spent for vaporization, which is negligible for the melting and ejection process

The absorptivity $\hat{\alpha}$ increases with workpiece thickness [21, 30]. This is the result of change in the angle of incidence due to change in inclination angle of the cutting front [31, 32]. The maximum absorptivity of iron ($\hat{\alpha} = 0.41$) is achieved at the angle of incidence of $\theta = 87.3^\circ$ (the corresponding angle of inclination of cut front is $\alpha = 2.7^\circ$) for the unpolarized CO₂ laser beam as shown in Fig. 2.5. The increasing effect of multiple reflections with an increase in workpiece thickness also enhances the beam absorption in the kerf [33].

2. the exothermic heat in reactive laser cutting

When oxygen is used as assist gas for cutting mild steel, significant heat is generated during the oxidation of iron as



The energy contributed by exothermic reaction becomes saturated with increase in pressure of gas flow (the number of pure metal and oxygen particles in the molten region) [34]. It is calculated as [29, 30]

$$P_r = \frac{w_k \cdot \rho_m \sqrt{2D_{\text{eff}} \cdot d \cdot v_m}}{A_{r,\text{Fe}}} \Delta H \quad (2.9)$$

$$P_r = \frac{\eta \cdot d \cdot w_k \cdot V \cdot \rho_m}{A_{r,\text{Fe}}} \Delta H \quad (2.10)$$

The contribution of exothermic heat to the total cutting energy is about 40 % [35–37], 55–70 % [38], and 50–56 % and is independent of the workpiece thickness calculated from [30] for cutting mild steels and 60 % for cutting stainless steel [37]. Both the exothermic heat and absorbed laser energy increase with cutting speed, but the percentage of exothermic heat to the total cutting energy decreases with increase in cutting speed [26]. Therefore, the cutting process is significantly enhanced in terms of lower laser power, low gas pressure, and higher cutting speed with oxygen as assist gas compared with nitrogen as assist gas [39]. Application of oxygen as assist gas allows cutting speeds that are 3–6 times higher than those in laser fusion cutting with inert gas [40, 41].

Not all the molten iron in the cutting front is oxidized [39], the percentage of melt film that is oxidized increases with decrease in cutting speed due to the thinner melt film and longer reaction time at low cutting speed. Only 30–35 % of iron that undergoes oxidation contributes to the total energy balance of laser cutting. The degree of oxidation is independent of the workpiece thickness [30]. But Ivarson et al. [37] believed 50 % of molten iron when cutting mild steel, 30 % of iron and 30 % chromium when cutting stainless steel are oxidized, and the majority of products of the exothermic reaction are FeO during cutting of mild steel, Fe₂O₃, and Cr₂O₃ when cutting stainless steel. The oxidation levels in the particles ejected from different parts of cut front are different because of the difference in their exposure times to oxygen (stages of oxidation) [42]. The oxide

melt, FeO, when cutting mild steel, is of low viscosity and low surface tension at temperature above 2,000 K and therefore is easily removed from the cutting zone by the mechanical action of the oxygen jet [24, 39], but the Cr_2O_3 formed when cutting stainless steel is of high melting point ($>2,700$ K), which increases the viscosity of melt and hinders the diffusion of oxygen into melt [36].

In the momentum balance,

F_o , the gas static pressure [29],

$$F_o = \frac{\pi}{2} d \cdot w_k \cdot p_g \quad (2.11)$$

F_n , the normal component of dynamic gas force [29],

$$F_n = \frac{\pi}{2} d \cdot w_k \cdot p_g \cdot v_g \tan \alpha \quad (2.12)$$

F_t , the tangential component of dynamic gas force [29],

$$F_o = 2\pi w_k \sqrt{d \cdot \rho_g \cdot \mu_g \cdot v_g^3} \quad (2.13)$$

F_a , the force acting on melt due to ambient pressure [29],

$$F_a = s \cdot w_k \cdot p_a \quad (2.14)$$

F_{st} , the surface tension force of melt [29],

$$F_{st} = \pi d \cdot \sigma \quad (2.15)$$

F_d , the dynamic force [29],

$$F_d = \frac{\pi}{6} w_k \cdot \rho_m \cdot v_m^2 \cdot s \quad (2.16)$$

F_m , the force due to the friction loss in the melt [29],

$$F_m = \frac{\pi}{2s} w_k \cdot d \cdot \mu_m \cdot v_m \quad (2.17)$$

2.3.2.2 Characteristics of Cut Front

Laser cutting is the process of formation and removal of the cut front. Therefore, its characteristics, such as temperature, angle of inclination, and flow rate, determine the cut quality. Hence, the effect of processing parameters on these characteristic must be fully understood.

Considerable efforts have been made to investigate the characteristics of cut front by in-process visualization and monitoring [25, 43–47], and theoretical and modeling analysis [29, 38, 48–54].

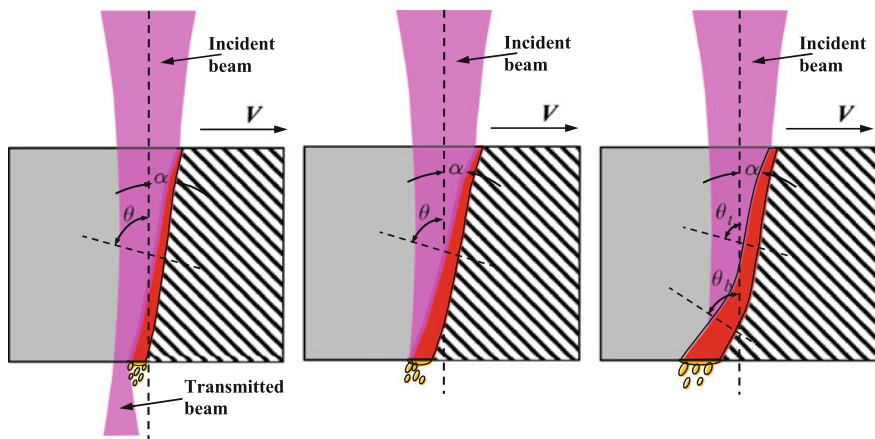


Fig. 2.9 Change in cut front with increase in cutting speed from (a) to (c)

Angle of Inclination of the Cut Front

It is found that the angle of inclination of the cut front increases with increase in cutting speed for both laser fusion cutting and reactive laser cutting [23, 29, 33, 45, 55], and the cut front becomes curved or kinked at high speeds [56] as illustrated in Fig. 2.9. The curved cut front at the lower part (Fig. 2.9c) with larger angle of inclination at high cutting speed is due to the lower laser irradiance in the lower part of the cut front than that in the upper part when the laser beam is focused close to the top surface of the workpiece [46] and will result in a change in melt flow direction [56].

The fraction of the laser beam incident on the cut front increases as the result of increase in angle of inclination of cut front at higher cutting speed.

In laser fusion cutting, the inclination angle increases with decrease in the linear energy density (either increase in cutting speed or decrease in laser power). An increase in the assist gas pressure increases the inclination angle probably due to the consequence of energy losses of higher removal of molten material [46].

Due to the increase in the Rayleigh length with shorter wavelengths for a Gaussian beam with $M^2 = 1$ as shown in Eq. (2.6), the angle of inclination of cut front in the case of fiber laser ($\lambda = 1.07 \mu\text{m}$) fusion cutting is larger than that of CO_2 laser beam fusion cutting, and the difference increases with increase in workpiece thickness [31].

The angle of inclination of the cut front reduces locally due to the formation of “shelves” on which melt accumulates and forms humps (as shown in Fig. 2.10). The accumulations of melt are produced periodically leading to melt flow instability [45].

In the remote fusion cutting without assist gas, the cutting front angle (complementary angle to angle of inclination α) decreases with increase in cutting speed and decrease in laser power, but is independent of the workpiece thickness.

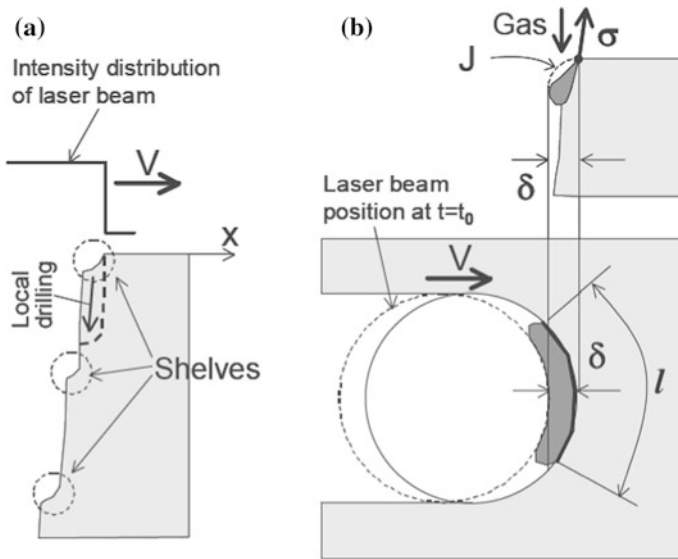


Fig. 2.10 **a** Side view and **b** top view of formation shelves and accumulation of melt (humps) (reprinted from Hirano and Fabbro [55] with permission. Copyright © Elsevier)

The maximum and the minimum cutting speeds are achieved at the minimum and the maximum cutting front angle, respectively, which are dependent on workpiece thickness [57].

The ratio of the area of cut front that is directly irradiated by the laser beam to the total area of cut front decreases with increase in the angle of inclination of the cut front after the full laser beam is incident on the cut front. The stable cut is still possible with the cut front not completely covered by the laser beam [56, 57].

If the angle of incidence is far from the Brewster's angle due to the change in angle of inclination of the cut front with increase in workpiece thickness and cutting speed, multiple reflections become significant and affect the cut process [33].

Temperature at Cut Front

In order to keep the cutting processing continuous, the temperature at the cut front has to be maintained above the material's melting point. The temperature at cut front is measured at approximately 2,000 K and maintained below boiling point of iron for reactive laser cutting of mild steel. FeO will not form (or, having formed, it will dissociate) if temperature in the melt exceeds the dissociation temperature (3,600 K), which makes the exothermic energy from the oxidation reaction not available as an energy input to the cut zone [39]. However, some modeling analyses show the melt temperature well above the boiling temperature [28, 38, 58–60].

Cut front temperature increases with laser power [48, 61] and cutting speed for both laser fusion cutting [29, 45] and reactive laser cutting [25, 39, 58, 62, 63]. This could be due to the following:

1. the greater beam coupling to the work material as the fraction of laser beam transmitted straight through the kerf with no heating effect decreases because of the increase in angle of inclination of the cut front [58];
2. increase in beam absorptivity with decrease in angle of incidence (increase in angle of inclination of the cut front) before reaching the Brewster's angle at higher cutting speed;
3. increase in exothermic heat in reactive laser cutting [26];
4. proportion of energy loss from cutting zone decreases with increase in cutting speed [26, 64].

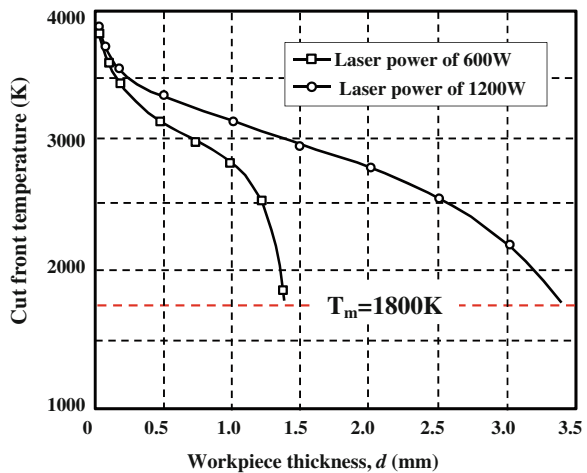
The temperature of the melt surface is not uniform through the thickness of workpiece. Higher temperature is achieved at the region closer to the bottom surface [62]. The melt surface temperature reaches the maximum temperature at the maximum cutting speed. The process breaks down at cutting speed higher than the maximum cutting speed because of abrupt drop in temperature of cut front at the region near the bottom surface [62].

It is reported that cut front temperature decreases with increase in workpiece thickness [48, 61]. The maximum thickness of a workpiece that can be cut at a given laser power is when the cut front temperature reaches the melting point as shown in Fig. 2.11 [48].

Cut front temperature is also found to be affected by beam polarization. It is higher with circularly polarized beam than with the radially polarized beam regardless of cutting speed [65].

It should be noted that the temperature of the melt surface fluctuates in reactive laser cutting because of oxidation dynamics [26].

Fig. 2.11 Effect of workpiece thickness on the cut front temperature (reprinted from Schuöcker and Abel [48] with permission. Copyright © SPIE)



The Melt Film Thickness

The melt film is very thin (of order of 10^{-5} m), and its thickness generally increased from the top to the bottom of the kerf [62, 66] as the melt accumulates at the bottom of cut front.

The melt film thickness, s , is formulated by Wandera et al. [54] for laser fusion cutting as

$$s = \frac{24V \cdot d^2 (\mu_g + \mu_m)}{\rho_g \cdot v_g^2 \cdot w_k^2} \quad (2.18)$$

and by Schuöcker et al. [34] for laser reactive cutting as

$$s = \frac{2k}{V} \left(1 - \frac{T_s}{T} \right) \frac{K_0 \left(\frac{V_{wk}}{4k} \right)}{K_1 \left(\frac{V_{wk}}{4k} \right)} \quad (2.19)$$

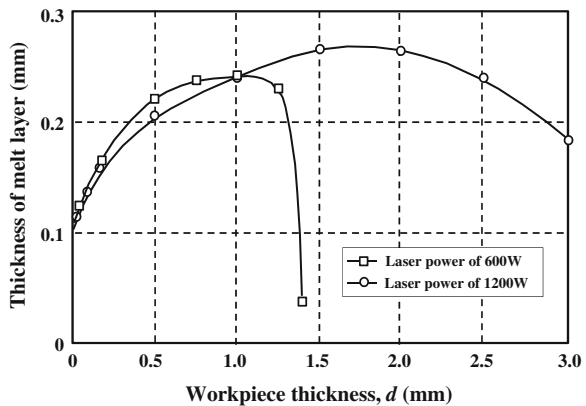
It clearly shows that the melt layer thickness increases with

- increase in thickness of workpiece as shown in Fig. 2.12 [48];
- increase in cutting speed [53, 56, 62, 67, 68] since more material is melted per unit time during cutting and higher mass flow rate at higher cutting speed, the thickness will be distorted at the region near the bottom surface when the cutting speed is close to the maximum cutting speed due to the inertial forces [62];
- decrease in gas velocity in laser fusion cutting [53].

However, Kaplan's analysis shows that the melt film thickness decreases with increase in workpiece thickness at a given cutting speed and laser power for laser fusion cutting as shown in Fig. 2.13a [29].

In reactive laser cutting of mild steel, a layer of FeO is formed on the surface of melt film, its thickness decreases with increase in cutting speed [69] and pressure

Fig. 2.12 Effect of laser power and workpiece thickness on melt layer thickness (reprinted from Schuöcker and Abel [48] with permission. Copyright © SPIE)



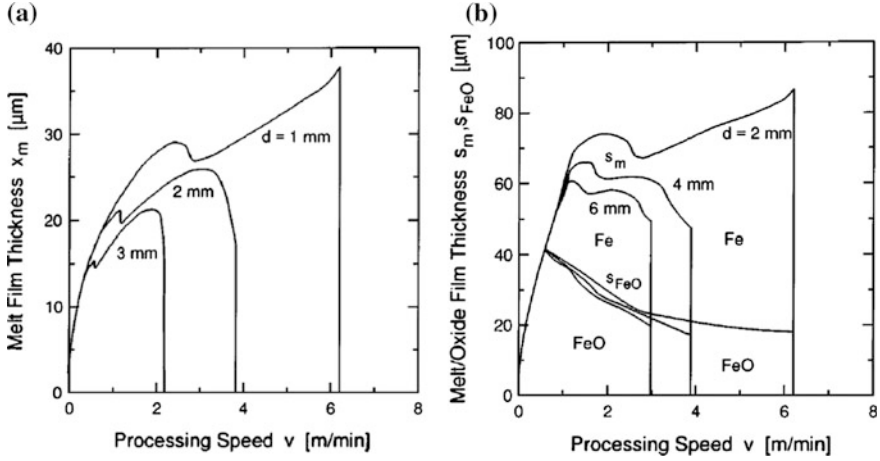


Fig. 2.13 Melt film thickness as function of cutting speed and workpiece thickness in (a) laser fusion cutting and (b) reactive laser cutting (reprinted from Kaplan [29] with permission. Copyright © American Institute of Physics)

of O_2 jet, but the fraction of oxide layer decreases with increase in cutting speed (as shown in Fig. 2.13b) and increases with increase in O_2 jet pressure [29].

The thickness of the melt film in reactive laser cutting fluctuates with the same pattern of the fluctuation of melt surface temperature [26].

The boundary layer thickness can be increased if shock structure in the assist gas flow field is formed inside the kerf because of the reduction in the flow velocity [70, 71].

In order to investigate the cutting conditions without evaporation, Olsen calculated and compared two melt film thicknesses, the maximum thickness of melt film in laminar one-dimensional melt flow (s_{HC}) and the minimum thickness of melt at the bottom of cut front by acceleration of the molten material (s_{ACC}) as [66]

$$s_{HC} = \frac{(T_E - T_M)K_m}{((T_M - T_0)C_p + L_M) \cdot \rho_m \cdot V \cdot \beta_B} \quad (2.20)$$

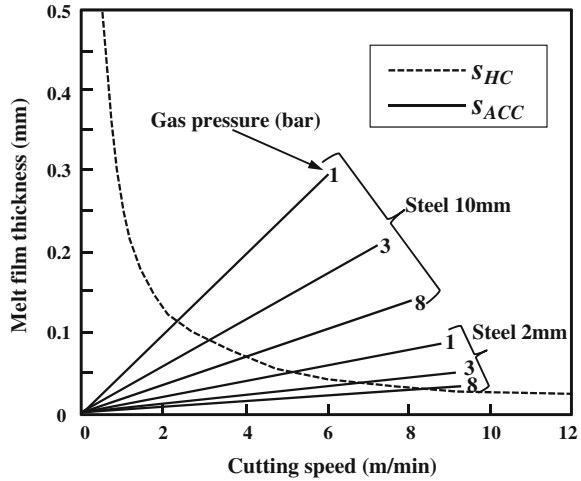
$$s_{ACC} = V \cdot d \sqrt{\frac{\rho_m}{P_g}} \quad (2.21)$$

Cutting without evaporation occurs when

$$s_{HC} > s_{ACC} \quad (2.22)$$

Thickness s_{HC} reduces with increase in cutting speed whereas s_{ACC} increases with increase in cutting speed and workpiece thickness, but decreases with increase in gas pressure as shown in Fig. 2.14.

Fig. 2.14 Melt film thicknesses of s_{HC} and s_{ACC} as function of cutting speed, gas pressure, and workpiece thickness (reprinted from Olsen [66] with permission. Copyright © SPIE)



Melt Flow Velocity

When the highest melt surface temperature is lower than the boiling temperature, the melt flows downstream in one dimension due to two driving forces acting on it by the momentum transfer of the pressurized gas flow in laser fusion cutting with high-pressure gas jet [50]:

1. pressure gradient of the gas flow
2. shear stress due to viscous friction within the boundary layer

Both mechanisms tend to remove the molten material in a direction parallel to the cutting front, and both contributions are of the same order of magnitude and increase with increase in gas velocity and angle of inclination of the cutting front [50].

However, the gas pressure is much lower in reactive laser cutting, the pressure gradient of the gas flow is negligible. The melt is considered to be removed primarily by shear stress due to the viscous friction [72, 73]

The maximum melt flow velocity, v_m , at the gas/melt interface is found in laser fusion cutting [54]:

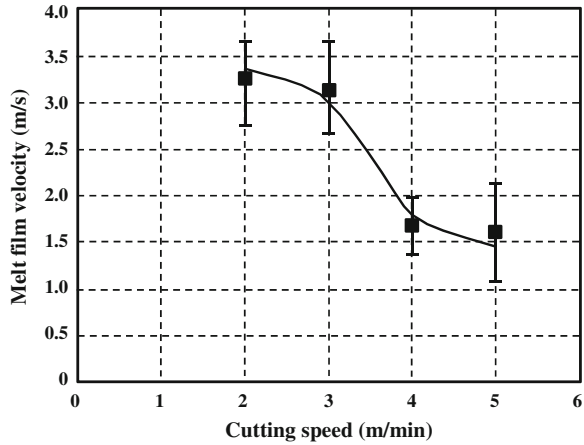
$$v_m = \left(\frac{1}{\mu_g + \mu_m} \right) \left(\frac{\rho_g \cdot v_g^2}{16d} \right) w_k^2 \quad (2.23)$$

in laser fusion cutting [74]:

$$v_m = \frac{\rho_g \cdot l}{24\mu_m} \left(\frac{F \cdot v_g}{H} \right)^2 w_k \quad (2.24)$$

and in reactive laser cutting [48, 61]:

Fig. 2.15 Velocity of melt film flow as a function of cutting speed in laser fusion cutting (reprinted partially from Hirano and Fabbro [45] with permission. Copyright © IOP Publishing Ltd)



$$v_m = \sqrt{\frac{\mu_g}{\rho_m} \frac{d}{s \cdot w_k}} v_g \quad (2.25)$$

From the above equations, it can be concluded that high velocity and density of gas is required to increase the melt flow velocity.

Increase in cutting speed results in increase in cut front temperature (reduction in viscosity of the melt), angle of inclination of cut front and melt film thickness, and slight reduction in kerf width [24, 29]. The combination of these effects leads to the reduction in melt flow velocity as show in Fig. 2.15 [45]. However, Chen et al. shows that the melt surface speed increases with cutting speed [67].

When the highest surface temperature (at the bottom part of front) exceeds the boiling temperature with increase in cutting speed, evaporation takes place, which

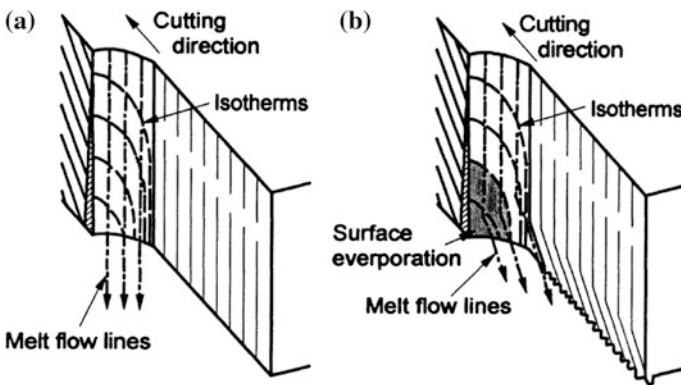


Fig. 2.16 Contours of isothermals and melt flows in (a) one-dimensional flow without evaporation and (b) two-dimensional flow with evaporation (reprinted from Olsen [66] with permission. Copyright © SPIE)

results in a local decrease in the melt thickness. If the evaporation is substantial, that is, when the evaporation pressure exceeds the cutting gas pressure locally, the melt flow will be forced not only downwards in the cut kerf (one-dimensional) but also around the laser beam (two-dimensional) as shown in Fig. 2.16 [66].

Mobility of Cut Front

Cut front does not always move at the same velocity with laser beam. It could move in front of or behind the laser spot depending on the heat balance affected by laser beam absorption, exothermic reaction, melt flow, and heat conduction. In the steady-state cutting, the melt front at a point moves at a velocity of V_M depending upon the angle between the cutting direction and the local normal to the melt front as [66]

$$V_M = V \cos \alpha \cdot \cos \beta \quad (2.26)$$

V_M is proportional to the corresponding local temperature gradients in the melt. The higher the V_M , the steeper temperature gradient is needed in the melt [66].

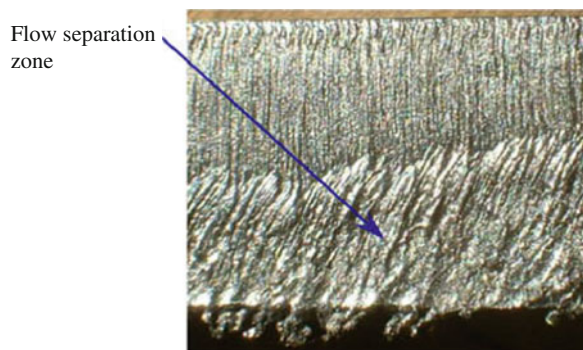
Difference in velocities of cut front and laser beam is also found during acceleration and deceleration in profile cutting, which is related to the issue of non-linear beam coupling to the workpiece [58].

Separation of Boundary Layer Flow

The melt velocity profile is dependent on the external pressure gradient through the workpiece thickness $\left(\partial P / \partial z\right)$ [54]:

- when $\partial P / \partial z = 0$, the velocity gradient gradually reduces to 0 at the outer edge of the boundary layer. The boundary layer is a perfect laminar flow;

Fig. 2.17 Poor surface quality at lower region of cut surface due to flow separation (reprinted from Kovalev et al. [75] with permission. Copyright © Elsevier)



- when $\partial P/\partial z$ increases to an extreme adverse pressure gradient $\partial P/\partial z \gg 0$, the velocity profile is significantly distorted at the kerf wall. The separation of flow occurs at the point of velocity gradient of zero, from which the boundary layer flow transitions into turbulent flow. The shear stress resulting from friction between the gas stream and melt is reduced significantly at the separation point [68].

When the depth of flow separation is smaller than the thickness of workpiece, rough surface finish at the lower region and strong dross attachment to the lower cut surface are produced as shown in Fig. 2.17.

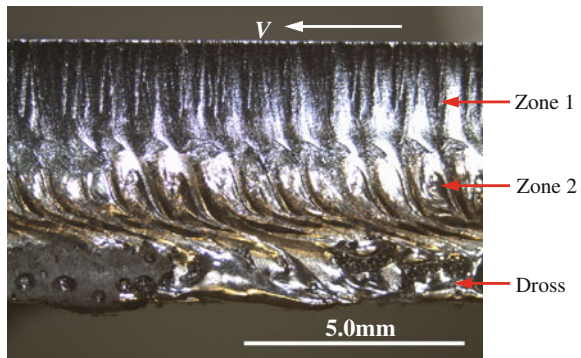
In order to maintain a high cutting quality, a laminar boundary layer melt flow must be maintained throughout the cut depth. Therefore, it is desired to have a depth of flow separation being larger or equal to the workpiece thickness to obtain clear cut. The depth of flow separation can be increased in laser fusion cutting [54] by:

1. increasing the gas pressure to reduce melt film thickness [75];
2. increasing nozzle diameter;
3. focusing the laser beam close to the bottom edge of the workpiece for thick workpiece with sufficient power intensity;
4. increasing melt surface temperature by increasing cutting speed and laser power;
5. increase in the kerf width [68].

2.3.2.3 Characteristics of Cut Surface

The characteristics of cut surface are important because the quality of the subsequent operations (such as welding) is strongly affected by the characteristics of cut surface, which are described as striation, dross as shown in Fig. 2.18, and heat-affected zone.

Fig. 2.18 A typical poor cut surface showing striations in zones 1 and 2 and dross produced in cutting mild steel by reactive laser cutting process



Striation

Striations are regularly periodic lines produced on cut surface (as shown in Fig. 2.18) during both laser fusion cutting and reactive laser cutting processes. The angle of the striations relative to the laser beam axis increases with increase in cutting speed.

Two different patterns of striation are observed on the cut surface when workpiece thickness is over 2 mm [24]. One is near the top surface adjacent to the cutting head with a relatively fine pattern (short wavelength) and another is at the lower part of the cut edge with a relatively coarse pattern (much longer wavelength). The two patterns are separated by a straight line extending in parallel to the surface of the workpiece [49]. The separation line is shifted toward the top surface of the sheet metal with increase in cutting speed [43].

The subsurface in the striation at zone 1 does not show resolidified microstructures [24, 43], but the striation at zone 2 shows the resolidified microstructures in its subsurface, which indicates that the striation at zone 2 is formed as a result of the turbulent melt film resolidification on the cut surface before it is ejected from the kerf.

Deep striation affects the quality of the cut surface (high surface roughness, geometry accuracy, etc.). Striation is characterized by its depth (surface roughness) and wavelength. It is found that striation depth (surface roughness) increases with increase in workpiece thickness [76] and oxygen jet pressure [26, 67, 77]

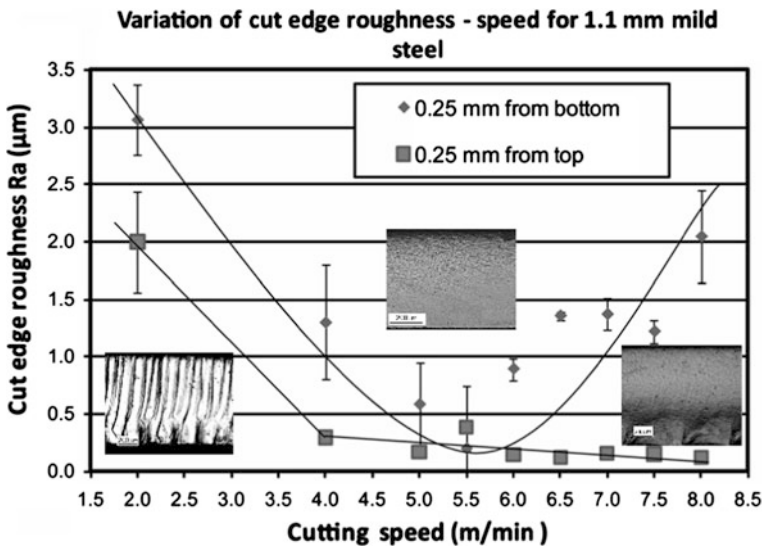


Fig. 2.19 Variation of surface roughness at 0.25 mm from top and bottom surfaces with cutting speed during fiber laser cutting mild steel with oxygen jet. Insert photographs were taken from the lower regions at cutting speeds of 2.0, 5.5 and 7.0 m/min, respectively (reprinted from Powell et al. [56] with permission. Copyright © Elsevier)

because of excessive oxidation and decreases with increase in cutting speed in reactive laser cutting [26, 67] and laser fusion cutting [45]. An optimum cutting speed exists for minimum surface roughness (striation-free) for reactive laser cutting of thin workpiece [56, 60, 78, 79] as shown in Fig. 2.19.

Change in the wavelength of striation pattern is controversial. Ivarson et al. [24], Chen et al. [67], and Schuöcker [49] reported that the striation wavelength gradually increases with increase in cutting speed at constant laser power when cutting mild steel with oxygen jet. Kaplan et al. [27], Poprawe et al. [43], and Ledenev et al. [80] concluded that the wavelength of periodic striations in zone 1 is independent of the cutting speed, but strongly correlates with the beam radius at the workpiece surface in reactive laser cutting of mild steel [27] and reduces with increase in gas pressure in laser fusion cutting [80]. Hirano et al. [45] found that the striation wavelength gradually decreases with increase in cutting speed during laser fusion cutting.

The formation of striation is the result of dynamic change in cut front thickness and temperature which can be brought by thermal dynamic instability (cyclical heating) or hydrodynamic instability (dynamic melt removal). There are several mechanisms for striation formation proposed as follows:

1. Thermal dynamic instability

The energy input fluctuates in laser cutting. It may come from (1) temporal fluctuations of laser power (either due to periodic absorption, periodic distortion of laser power, and coupling of reflected laser radiation with laser resonator) [23, 49]; (2) cyclical burning in reactive laser cutting due to oxidation dynamics at low speed [24–26, 28, 56, 59, 60]. The temporal fluctuations of laser power can be minimized by stabilizing laser output power and mode [23]. Instability in thermal dynamic results in localized heating and intermittent melting in the kerf front in the region where the kerf front wall becomes nearly vertical [45].

- Cyclical burning in reactive laser cutting

This was first observed by Arata et al. [25]. A sideways burning cycle of ignition–burning–extinction (as shown in Fig. 2.20a) occurred in reactive laser cutting when the cutting speed is below the velocity of the oxidation front, a critical speed at typically 2 m/min (or 33 mm/s) for mild steel. Oxidation front moves at velocity of V_M faster than laser beam velocity of V during burning process (process II), but slower during extinction process (process III).

The oxidation when the cutting speed is below the velocity of the reaction front is a dynamic process. When the oxidation front moves well ahead of laser spot (in extinction process III) due to the release of exothermic heat during burning process II, it increases the instantaneous thickness of FeO and decreases the oxygen gradient as shown in Fig. 2.20b. The reduction in oxygen gradient with growth of liquid volume (thickness) during burning process contributes to the extinction. Reignition occurs after the molten layer is removed from cutting zone and laser beam recatches the cutting zone [24].

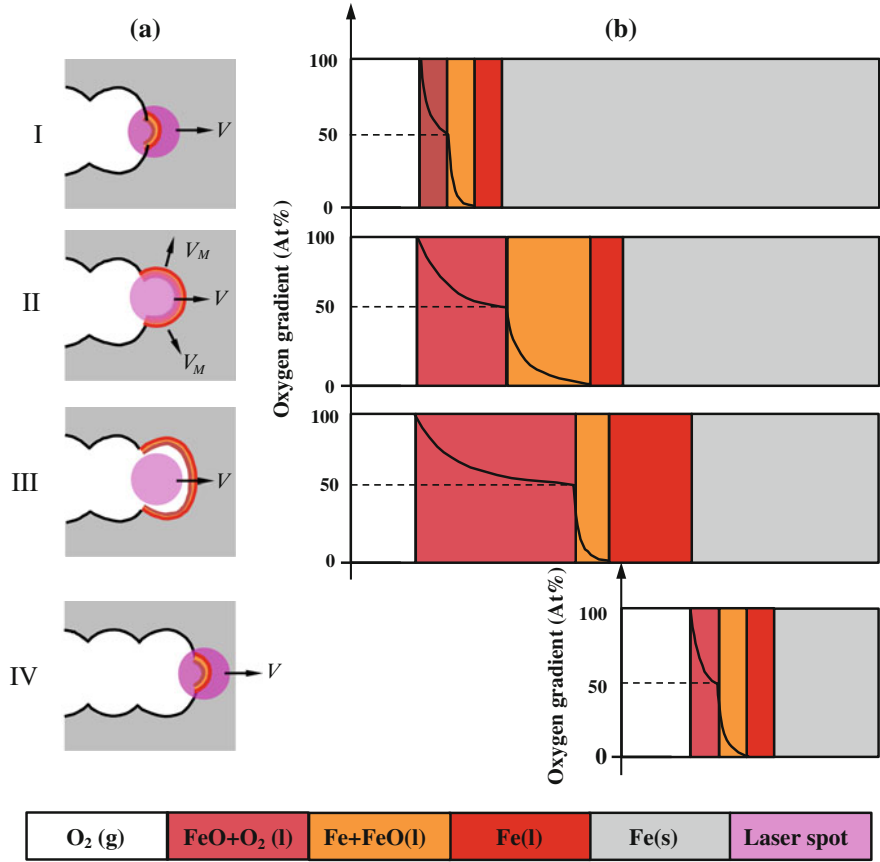


Fig. 2.20 Schematic illustration of (a) top view, (b) side view and oxygen gradient across melt film during a cycle of (I) ignition, (II) burning, (III) extinction, and (IV) reignition during formation of striation by sideways burning (drawn in reference to [24, 25])

2. Hydrodynamic instability

The ideal flow of the melt out of kerf is laminar flow with uniform thickness and temperature. However, the melt layer oscillation which leads to striation formation at high cutting speed with inert gas could occur due to:

- fluctuation in gas flow (to be discussed in Section “Assist Gas” in details) [49];
- transition of gas flow from laminar to turbulent due to increase in angle of inclination of cut front, which could result in reaction energy intensity instability and metal removal instability [81];
- increase in molten layer thickness, which may lead to spatial distortion on the cutting edge due to liquid oscillation and turbulent flow near the bottom surface [56, 81];

- the onset of ripple formation on the cut edge is caused by the time-dependent movement of the width of the cutting front as a response to fluctuations of the processing parameters [52];
- melt flow transition from one-dimensional to two-dimensional melt flow due to evaporation, which causes liquid layer oscillation [23, 81];
- melt flow is hydrodynamically unstable if the flow is dominantly driven by pressure gradient of the gas flow [53];
- cyclical formation, growth of liquid droplet, which is separated (broken away) from the melt layer when the weight of the forming droplet and the melt flow's starvation pressure overcome the surface tension [82] or the critical radius of droplet is reached [80], the critical drop size is reached when the balance between capillary forces and forces exerted on the melt by the gas stream in the vicinity of the upper edge of the cutting front is achieved [83];
- the periodic growth of the humps (as shown in Fig. 2.10), which start to flow when the gas force exceeds the surface tension force [45];

Because the cut surface quality is important in some applications, the following strategies have been developed to reduce or eliminate the striation formation:

- High-pressure cutting, where the high gas pressure efficiently ejects the melt film, resulting in a thin melt film. Thereby, the amplitudes of the melt film oscillations are limited [23].
- Low pressure cutting, applying subsonic gas jets, where the melt film thickness is relatively large, but the smooth gas flow reduces the melt film oscillations [23].
- The melt flow dominantly driven by shear force is stable and can be achieved by either decreasing cutting speed or increasing gas velocity. This is proven only for the striation formation at high cutting speed [53].
- Cut at speed higher than the speed of combustion-front motion [25, 72].
- Carefully control the pulse frequency of laser beam (in the order of twice the striation frequency under the CW laser cutting condition) [84, 85].
- Material is mainly removed by vaporization due to the suppression of melt flow formation, which can be achieved with high brightness and the small beam divergence of the fiber laser [28, 60, 79] or pulsed laser with high average power and high pulse repetition rate [86].

Dross

When the momentum of molten layer transferred from the pressurized gas is higher than the surface tension force, clear cut is made by removing the molten metal from the bottom of kerf [87]. Formation of dross at the bottom cut edge is the result of high surface tension and viscosity of the melt film. Therefore, the melt cannot be expulsed completely from the bottom of the kerf.

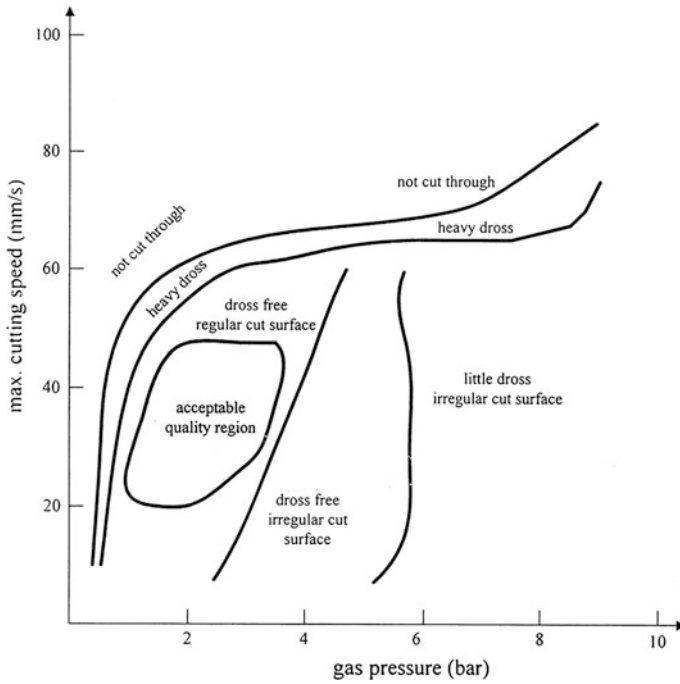


Fig. 2.21 Process window for high-quality cut in reactive laser cutting mild steel with thickness of 3 mm (reprinted from Chen [90] with permission. Copyright© Elsevier)

Similar to striation formation with respect to cutting speed in reactive laser cutting, there is an optimal cutting speed to achieve minimum dross cut as shown in Fig. 2.21. The larger amount of dross produced at cutting speed below or above this optimal cutting speed is due to the solidified large amount of backward flow of melt and strong disturbance of the melt flow [88], respectively.

In order to deform, break up, or detach the melt droplet at lower cut edge by shear action of the gas to achieve a dross-free cut, the Weber number (We) of the melt in the lower part of the cutting front must exceed a critical value [46].

Dross formation when cutting thick workpiece when laser beam is focused at the top surface is due to insufficient energy. This leads to difficulty in separating melt from the lower cut edges. Increase in laser power can eliminate the dross at the expense of poor cut quality because of poor beam-mode quality of CO_2 laser at high laser power [89].

The dross attachment on the lower cut edge can be reduced by increasing the depth of flow separation as discussed in Section “[Separation of Boundary Layer Flow](#)”.

Melt flow velocity increases and the melt film thickness decreases with increase in assist gas pressure or kerf width. This leads the boundary layer separation point moving down the cut kerf. Therefore, the dross attachment on the lower cut edge

reduces with increase in assist gas pressure and cut kerf width in laser fusion cutting [54, 90].

During reactive laser cutting of thick workpiece, the oxygen jet is kept at low pressure (maintaining the gas flow developed in the cut channel to be subsonic, transonic, or slightly supersonic) in order to control the regime of metal burning. The ambient air is entrained in the oxygen flow [73, 91], which increases the impurity of oxygen jet and retardation of oxidation reactions.

Vortex is formed when pressure in the peripheral nozzle is lower than a critical value. The vortex flow can entrain and accumulate the liquid melt, which restrains its removal from the cut even induces the reverse motion of the melt and is responsible for slagging at the bottom of the cutting kerf and adhesion of dross [73, 75].

Heat-Affected Zone (HAZ)

Laser beam cutting is a thermal process. The heat conduction loss to the surrounding solid part results in temperature rise in the subsurface at a depth from the cut surface [32], which may results in change in the microstructure and phase composition such as martensitic transformation, change in grain size, and carbide formation in the HAZ. These changes are normally undesirable because of higher tendency of cracking, surface hardening, decrease in weldability, corrosion resistance, and fatigue life [87, 92, 93].

The width of HAZ increases with increase in workpiece thickness because of the higher heat conduction loss when cutting thicker workpiece [94].

Increase in cutting speeds causes the energy density to decrease and less heat conducted to the bulk workpiece resulting in reduction in thickness of HAZ layers if no resolidified material is attached to the cut edge [93].

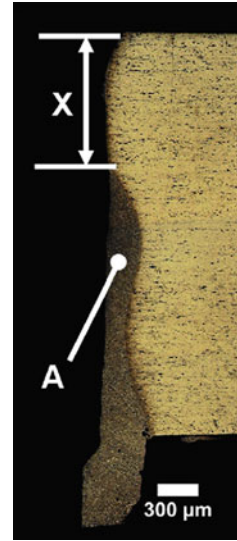
The width of HAZ is affected by the type of cutting nozzles used. The HAZ obtained when using conical coaxial cutting nozzle is larger than that obtained by using the supersonic cutting nozzle. The reduction in HAZ by using Laval nozzle is more significant when cutting thicker workpiece [94].

The thickness of HAZ layer decreases with the increase in gas pressure during laser fusion cutting due to the effective removal of the melt from the laser-material interaction region by the strengthened shearing stress of the gas flow and the strengthened cooling effect [93].

The melting point of some products of the chemical reaction during reactive laser cutting is very high, for example, 2,017, 2,230, and 2,435 °C for Al_2O_3 , AlN and Cr_2O_3 [36, 94], respectively. They are repeatedly fractured due to the turbulent nature of the melt flow out of the cut zone and dispersed in the melt, which results in increase in the viscosity and surface tension of the melt. Therefore, the velocity of melt flow is reduced, which causes the larger HAZ [94].

The dross attached at the lower cut edge is the melt that is not completely extracted by the assist gas from the cut kerf and solidifies on the cut edge. This produces significant HAZ at the lower region of cut edge as shown in Fig. 2.22.

Fig. 2.22 HAZ at the lower region of the cut surface due to heat by the adhered resolidified layer (reprinted from Riveiro et al. [95] with permission. Copyright © Elsevier)

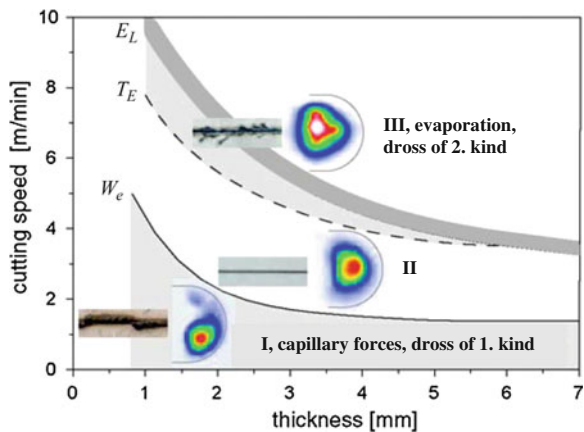


The amount of resolidified material on the cut surface increases with increase in laser power and cutting speed because of the higher rate of melting and higher recoil pressure which expels more molten material backwards toward the cutting front [46]. The proportion of distance X (the distance from the upper surface of the plate up to the beginning of the HAZ) to the thickness of workpiece increases with increase in laser power, gas pressure [95], and optimum pulse frequency [96].

HAZ due to the heat conduction can be reduced when cutting with pulsed laser at high pulse frequency [93, 97] and low duty cycle [97], because of lower heat input.

However, the HAZ due to the adhesion of resolidified melt layer on the cut surface during pulsed laser cutting of ceramics increases with increase in pulse frequency because of the thicker resolidified layer at the end of laser pulse [22].

Fig. 2.23 Ranges of cutting speed and cut quality (reprinted from Poprawe and König [43] with permission. Copyright © Elsevier)



The plasma formation also increases the HAZ, and this is more significant when cutting titanium alloys compared with mild steel because of the significantly lower thermal conductivity of titanium alloys [98].

2.3.2.4 Processing Parameters

Cutting Speed

Laser cutting can be conducted in a wide range of cutting speeds, which strongly depends on the workpiece material and its thickness as shown in Fig. 2.23 [43]. The maximum cutting speed decreases with increase in workpiece thickness. There are three regions in Fig. 2.23 with respect to cutting speed for laser fusion cutting [43] as follows:

- In Region I at low cutting speed range where Weber number $We \approx 1$, the capillary forces become comparable with the inertia of the melt. Therefore, the melt flow does not separate completely from the cut kerf and dross attachment occurs at the bottom of cut edge.
- In Region III at high cutting speed range from T_E where vaporization of melt film occurs to the maximum cutting speed limited by energy (E_L) for a given thickness of workpiece, melt flow is interrupted by the onset of vaporization. The melt flow becomes two-dimensional due to the vapor pressure (as shown in Fig. 2.16) leading to rough cut at the lower region of the cut surface [66].
- In Region II at the middle cutting speed range, workpiece is melted and melt flow is stable one-dimensional.

The maximum cutting speed is limited by the workpiece thickness and laser power [43]. At a given laser power, the maximum cutting speed decreases with workpiece thickness. It should be noted that the evaporation contribution to the maximum cutting speed reduces with increase in workpiece thickness [48].

The optimal cutting speed is defined as the highest speed for the best quality cut. It is generally 80–90 % [99] or between 70 and 80 % [78] of the absolute maximum cutting speed.

The maximum cutting speed without evaporation can be theoretically calculated by combining Eqs. (2.20), (2.21), and (2.22) as follows [66]:

$$V_{\text{Melt}} = \sqrt{\frac{(T_E - T_M)K_M\sqrt{P_g}}{((T_M - T_0)C_p + L_M)\sqrt{\rho_m^3} \cdot d \cdot \beta_B}} \quad (2.27)$$

The empirical relationship between incident laser power (P), cutting speed (V), thickness of workpiece (d), and width of kerf or diameter of laser spot (w_k) can be written as follows:

$$P = B \cdot w_k^{0.01} d^{0.21} V^{0.16} \quad (2.28)$$

which is valid to a high degree of accuracy for laser cutting of different workpiece materials (steel, glass, plastic, wood PVC, etc.) with variation of B only [100, 101].

Laser Beam

Cutting performance is strongly affected by the characteristics of laser beam, which can be operated with different wavelengths, polarizations, and modes, focused with different optics and different focus position relative to workpiece surface.

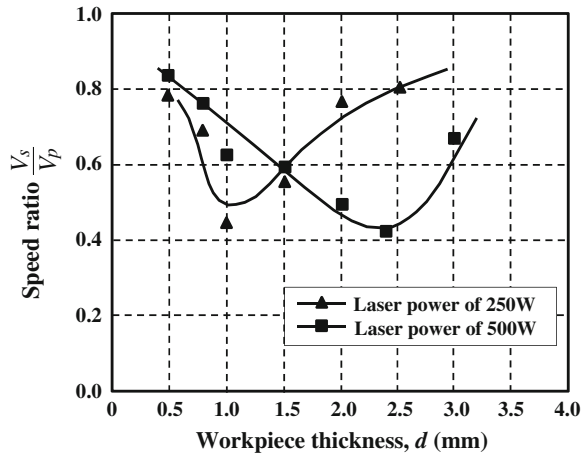
Polarization of Beam

Due to the difference in absorption with the polarization and incident angle for linearly polarized laser (such as CO₂ laser in Fig. 2.4), the maximum cutting speed when the cutting direction is parallel to the plane of polarization (V_p) is higher than the maximum cutting speed when the cutting direction is perpendicular to the plane of polarization (V_s). Therefore, the plane of polarization should be parallel to the cutting direction for straight-line cut, but a circularly polarized beam should be used for profile or contour cutting in order to avoid the directional effect [6, 102].

Since the p-polarized laser beam is almost completely absorbed at the Brewster's angle (about 87.3° as shown in Fig. 2.4) and change in angle of inclination with cutting speed (as shown in Fig. 2.9), the fastest cutting speed can be achieved with inclination angle of cut front at 2.7° [32].

Because the difference in absorptivity between p-polarized beam and s-polarized beam changes with the workpiece thickness as the change in angle of incidence with workpiece thickness, the ratio of maximum speeds, V_s/V_p , decreases with increase in workpiece thickness, reaches a minimum at a critical thickness,

Fig. 2.24 Effect of workpiece thickness on the maximum cutting speed ratio with respect to beam polarization (reprinted from Lepore et al. [103] with permission. Copyright © Elsevier)



and then increases with increase in workpiece thickness (as shown in Fig. 2.24). The maximum effect of beam polarization is achieved at the critical workpiece thickness. This could be due to the fact that the contribution of exothermic heat is stronger when the workpiece thickness is larger than its critical value during reactive laser cutting [103] or the angle of incidence is equal to Brewster's angle at the critical workpiece thickness.

Muys et al. [104] conducted simulation to verify a model proposed by Niziev and Nesterov [105] and conclude that radial polarization of laser beam can either increase cutting speed for the same thickness or increase the cutting depth for the same laser power.

Wavelength of Laser Beam

It has been reported that the cutting with fiber laser is more effective because of the smaller severance energy (linear energy per unit sheet thickness) during fusion cutting with fiber laser compared with CO₂ laser [21]. Cutting speed is remarkably increased with high-brightness fiber laser compared with CO₂ laser in cutting thin workpiece [21, 106, 107]. The cut quality with fiber laser is worse when cutting workpiece thicker than 5 mm as shown in Fig. 2.25.

However, the cut quality and cutting performance during reactive laser cutting of steel sheet with thickness up to 20 mm are not significantly affected by the wavelength [107], which indicates the contribution of oxidation in reactive laser cutting is more pronounced than the contribution of the characteristics of laser.

The difference between fiber and CO₂ lasers is their wavelength and absorption behavior. The shorter wavelength of fiber laser enables it to be focused for longer distance (longer depth of focus as calculated by Eq. (2.6)) which provides high energy intensity to cause the workpiece vaporization and create a keyhole [108].

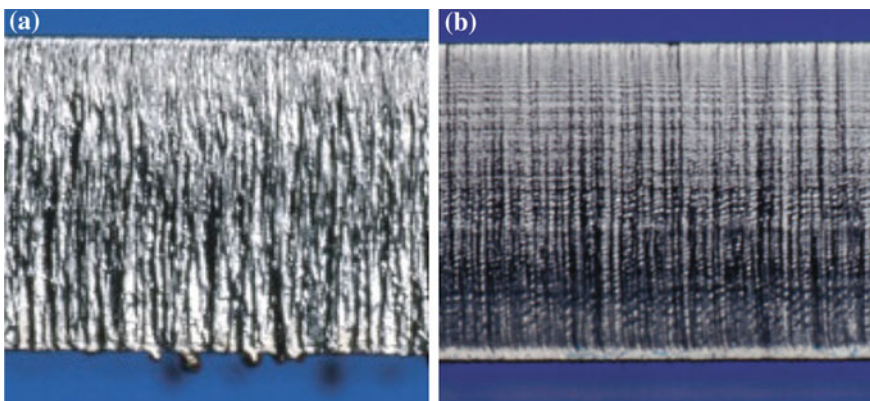


Fig. 2.25 Cut surface of 4-mm stainless steel with laser fusion cutting by (a) fiber laser and (b) CO₂ laser at power of 2.5 and 3.0 kW, respectively (reprinted from Poprawe et al. [107] with permission. Copyright © Elsevier)

Almost complete melt ejection can be achieved in thin sheet by the vapor pressure gradient, which leads to clear cut [107]. The smaller Brewster's angle with fiber laser (79.6°) compared with CO_2 laser (87.3°) as shown in Fig. 2.5 enables the better laser absorption at larger angle of inclination of cut front (with higher cutting speed), which can be achieved with thin workpiece sheet [31]. In order to achieve the better efficiency in fiber laser cutting thick sheet, the inclination angle of cut front needs to be increased, which can be achieved by adapting the beam oscillation strategy with a longitudinal beam deflection during the cutting process [31].

The more efficient cutting and higher cutting speed with fiber laser is attributed to the better beam coupling and increased laser beam absorption as result of multiple reflections [109, 110], which is more severe with thicker workpiece. The multiple reflection contribution typically starts at the depth of 1–2 mm below the surface and causes the curved and kinked cut front as shown in Fig. 2.9 [56]. It destabilizes the lower cutting zone and leads to coarser striations [109].

Because of the narrower kerf with fiber laser due to its longer depth of focus [31], the gas pressure reduced significantly down through the cut kerf, which lowers the melt flow out of the kerf [111]. Multiple laser beams were developed by Olsen et al. [108] when cutting with fiber laser. The laser intensity is tailored as a central high-intensity melt beam followed by several beams in an appropriate beam pattern, which guide the melt flow out of the cut kerf by creating local evaporation as in the keyhole. Cut quality is improved over a wide range of cutting speeds, and dross-free cut is achieved with this beam configuration compared with single beam cutting.

Pulsed Laser Beam

Pulsed laser provides a high instantaneous power for a period of pulse duration and followed with a period of power off. This offers some benefits in laser materials processing compared with CW lasers [5]:

1. The high pulse peak power results in improved laser coupling for some materials with high reflectivity such as aluminum alloy.
2. The temporal limitation in energy input leads to reduced heating of workpiece and small depth of heat conduction into the workpiece. This is more prominent for materials with low thermal conductivity such as titanium and nickel alloys.

The small heat input with pulsed laser cutting also benefits the reduction in stress-induced cracking in the brittle materials such as ceramics.

These advantages are achieved at the cost of reduced cutting speed at low pulse frequency compared with CW laser cutting [5, 112].

Under the optimized conditions (pulse frequency range of 400–600 Hz and power on-time/off-time ratios of between 5 and 9 to 1), the optimal cutting speed with pulsed laser is higher than that with CW laser by 10 % or more at the same average laser power due to the higher temperature in the cutting zone associated

with higher peak laser power in reactive laser cutting mild steel. Furthermore, fluctuation in maximum cutting speed induced by oxygen shock wave during reactive laser cutting is smaller when using pulsed laser compared with CW laser [113].

Laser spot overlap is important for pulsed laser cutting. The spot overlap required for cut decreases with increase in pulse energy and a minimum of 45 % spot overlap is required for clearly through cutting. The kerf width increases and surface roughness decreases with increase in spot overlap [114].

For a given pulse energy, it was found that the maximum cutting speed increases with reduction in pulse duration for cutting nickel-based superalloy [114] as the higher peak laser power with shorter pulse duration. Bicleanu et al. [115] and Lee et al. [116] reported that cutting speed increases with increase in pulse width in pulsed Nd:YAG laser cutting of mild steel and stainless steel.

During pulse mode laser cutting, melt ejection occurs in each laser pulse on-time while melt front cools during pulse off-time. Minimizing dross formation can be achieved in pulsed mode cutting by using low duty cycle pulses which not only provided low heat input that reduced the quantity of melt formed but also imparted sufficient cooling between two successive laser pulses which prevented over-heating of the cut front [97].

Cut quality is reported to be improved by using pulsed lasers [43, 84, 85]. The laser pulse duration (t_{on}) has to be matched to the typical time (d/v_m) for the propagation of a melt perturbation along the whole cut front down the workpiece thickness in order to allow the melt produced in one laser pulse to be ejected

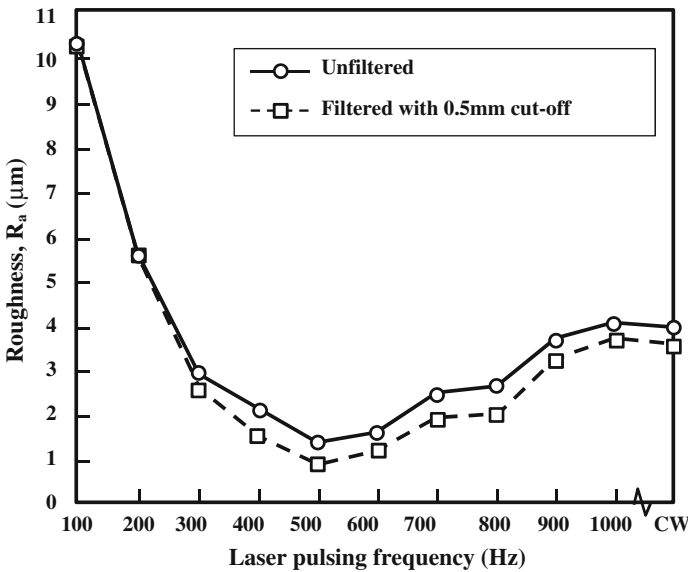


Fig. 2.26 Effect of pulsed frequency on the cut surface roughness in laser cutting mild steel with oxygen (reprinted from King and Powell [84] with permission. Copyright © Elsevier)

completely for dross-free cut. The cycle time $t_{\text{on}} + t_{\text{off}}$ has to meet the time-averaged energy balance [43].

The interference of perturbation dynamic induced by pulsed laser with the melt flow dynamics enable to minimize the striation formation. The reduction to approximately one-quarter of surface roughness obtained under CW cutting is achieved at the pulse frequency between 400 and 700 Hz (as shown in Fig. 2.26). Higher roughness in the pulsed ranges below and above this range is attributed to the small laser spot overlap and diminished effect of individual laser pulses, respectively. The surface roughness is not significantly influenced by pulse length (mark-space ratio) at the optimum frequency range [84].

The difference between the unfiltered and filtered roughness curves in Fig. 2.26 shows that contribution of a low-frequency periodic roughness (excluded with 0.5-mm cutoff by a phase-corrected high-pass filter) with respect to laser pulsing frequency.

Recrystallization in the heat-affected zone leads to deterioration of surface characteristics. The width of recrystallization zone can be reduced with longer pulsed width at a given pulse energy due to the lower peak power with longer pulsed width [117].

During the pulsed laser cutting of ceramics, the melt is predominantly removed by the momentum transfer from the pressurized gas jet at high pulse frequency and recoil pressure at low pulse frequency [22].

Focusing Laser Beam

Kerf width increases if the focus of the laser spot shifts from the workpiece surface. Minimum kerf width is achieved when the laser spot focus is on the workpiece surface [111]. Wider kerf width can be obtained when laser beam focuses either above the workpiece top surface or close to the bottom surface of the workpiece. This enhances the melt flow velocity in the cut kerf so that the melt flow clears the bottom cut edge before flow separation occurs and with minimal dross attachment on the lower cut edge when cutting thick workpiece provided the energy intensity is sufficient [54].

Due to the relative wider kerf width during laser reactive cutting as the result of sideways burning and low viscosity of melt with FeO, laser beam is recommended to focus at top with oxygen-assisted laser cutting [89].

For cutting thin metal sheet, the laser focus is recommended to be on the top surface of the workpiece to get narrow kerf. However, the melt in narrow kerf is difficult to be removed when cutting thicker workpiece. Therefore, it is suggested that laser beam is focused at bottom of thick stainless steel with nitrogen as assist gas to avoid burr formation [43, 89], with a disadvantage of increased roughness at the lower cut edge [43].

With a single transmitting or reflecting optical element, a laser beam can be focused at two fixed focal points at two different positions, spaced from each other in the direction of material thickness. The concentric circular center surface areas of the optics create a focal point near the bottom surface of workpiece. The amount

of laser power focused near the bottom surface of workpiece depends on the diameter of this area. The outer ring area of the optics focuses the remained laser power close to the top surface of the workpiece. The possible thickness capable of being cut with a certain laser power level increases with application of dual focus lens [89].

The cutting speed increases by 23 % and kerf width reduces by 30 % with more perpendicular edges and less dross by using dual focus lens in cut medium section stainless steel with nitrogen compared by using single focus lens. This is attributed to the fact that a long depth of partially focused collimated beam at above and below the upper focal position. This deep-collimated beam increases temperature of the melt at the central sloped cutting zone high enough (below boiling point) to melt the material in the area is not directed irradiated by laser beam, which leads to increase in melt viscosity [118].

Longer focal length is found to reduce the maximum cutting speed by a factor ranging from 1.2 to 2.5 when cutting aluminum alloys [95]. This result can be attributed to a reduction in the power density on the cutting front as the result that spot size increases with increase in focal length.

Assist Gas

The functions of assist gas during laser cutting are to [119]:

1. protect the workpiece from undesirable reactions with the ambient gas and cool the hot cut zone by the forced convection;
2. remove the molten material from cutting front through the narrow kerf to keep the cutting process going. The flow need to be directed with a major component of its velocity in the direction of the expulsion;
3. provide exothermic heating by chemical reaction if reactive gas used.

Table 2.4 Chemical reactivity of common used gases with the common metals

	O ₂	N ₂
Fe	Fe + 1/2O ₂ = FeO + 275 kJ/mol (at 2,000 K) [37] 4Fe + 3O ₂ = 2Fe ₂ O ₃ + 822.2 kJ/mol ^a [156] 3Fe + 2O ₂ = Fe ₃ O ₄ + 1,117 kJ/mol ^a [155]	
Al	4Al + 3O ₂ = 2Al ₂ O ₃ + 1,670 kJ/mol ^a [156]	Al + N=AlN + 1050.4 kJ/mol (at 1,103 K above) [157]
Ti	Ti + O ₂ = TiO ₂ + 912 kJ/mol ^a [156]	2Ti + N ₂ = 2TiN
Cr	2Cr + 3/2O ₂ = Cr ₂ O ₃ + 1163.67 kJ/mol (at 2,000 K) [37]	
Ni	Ni + 1/2O ₂ = NiO + 244 kJ/mol ^a [156]	
Cu	2Cu + 1/2O ₂ = Cu ₂ O + 166.7 kJ/mol ^a [156] Cu + 1.2O ₂ = CuO + 155 kJ/mol ^a [156]	

^a at 293 K for comparison

Table 2.5 Comparison of properties of inert gases for laser fusion cutting (reprinted from Rao et al. [97] with permission. Copyright © Elsevier)

	Ar	He	N ₂
Stagnant gas pressure (MPa)	0.6	0.6	0.6
Gas density (kg/m ³)	1.3038	0.1306	0.9776
Specific heat capacity (J/kg K)	520	5,200	1,183
Thermal conductivity (W/m K)	0.0452	0.3765	0.0738
Viscosity (μPa s)	58	48.3	44
Critical gas velocity (m/s)	280	884	322
Shear stress (N/m ²)	850	1,390	800
Heat transfer coefficient (W/m ² K)	2,080	10,680	3,690

The cooling of the melt due to the gas jet is shown to be negligible compared to the incident laser beam power [50].

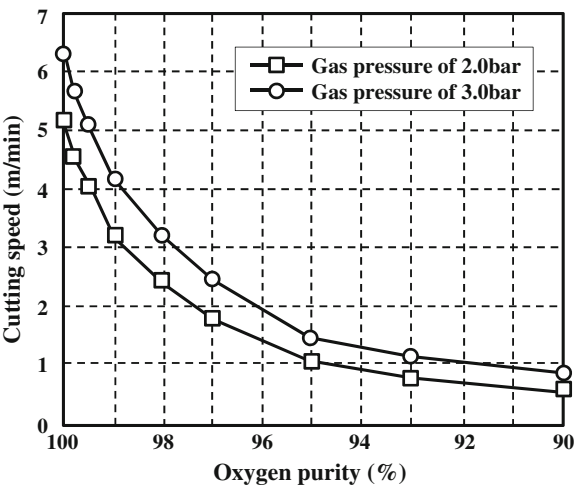
These functions are heavily dependent on the nature, pressure, and purity of the assist gas.

Gas Nature

The chemical reactivity of the commonly used gases for laser cutting is listed in Table 2.4. In addition to oxygen, nitrogen is chemically reactive with aluminum and titanium.

The properties of inert gases for laser fusion cutting are listed in Table 2.5. Helium shows the highest values of critical gas velocity, shear stress, and convective heat transfer coefficients.

Fig. 2.27 Effect of oxygen purity on cutting speed during cutting 2.0-mm-thick mild steel at CO₂ laser power of 800 W (drawn in reference to [99])



Gas Purity

Contamination of the inert gas only causes degradation of the cut surface, such as dross size, oxidation, or nitriding of the cut face. Cutting mild steel with mixture of two inert gases does not show significant difference with pure inert gas in cutting speed and dross formation at low gas pressure [41]. However, the impurity in oxygen significantly affects the cutting process.

The cutting performance strongly depends on the percentage of impurity in oxygen gas jet but not on the type of impurity gases, no dross-free cut can be obtained at oxygen level lower than 75 % in cutting mild steel of thickness of 3 mm with laser power of 1.5 kW and gas pressure of 2 bar [41].

The cutting speed is very sensitive to the oxygen purity at high purity level (99.998–95 %), 2 % of impurity is found to reduce the optimal cutting speed by more than 50 %. Cutting speed is not significantly affected by further decrease in oxygen purity from 95 to 90 % (as shown in Fig. 2.26) because the heat contribution by oxidation reduces with reduction in oxygen purity [99].

The oxidation is significantly reduced by the formation of a boundary layer at the gas–liquid interface in which the impurity gas is accumulated. This layer acts as a barrier to inhibit the oxidation reaction by lowering the oxygen diffusion rate in this layer [26, 99]. The thickness of the boundary layer can be reduced by increasing the gas pressure. Therefore, the cutting speed is increased by increase in gas pressure at the same oxygen purity level as shown in Fig. 2.27.

Reduction in oxygen purity also significantly reduce the critical cutting velocity above which oxidation is stable without the cycle of ignition-burning extinction [59].

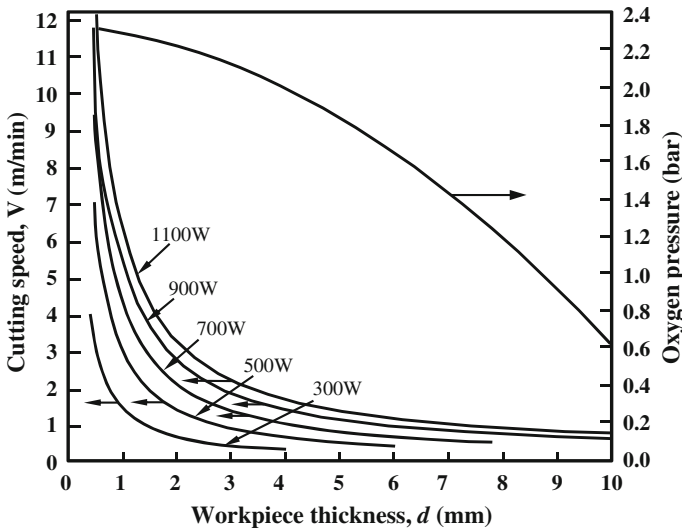


Fig. 2.28 Dependence of cutting speed and optimum oxygen pressure on workpiece thickness for CO₂ laser cutting steel (reprinted from Schuöcker [4] with permission. Copyright © Taylor & Francis)

Gas Pressure

The gas pressure does not show a significant influence on the maximum cutting speed but does have a significant effect on the quality of the cut edge in the laser fusion cutting process [33].

Increase in gas pressure with workpiece thickness (minimum of 8 bar for cutting stainless steel with nitrogen) is required to effectively remove the melt from kerf when cutting with inert gas. However, the gas pressure should be reduced (maximum of 6 bar when cutting mild steel with oxygen) with increase in workpiece thickness when cutting with reactive gas in order to control the cut surface quality as shown in Fig. 2.28 [4, 68, 120].

There are two optimum oxygen pressure ranges to obtain the good cut quality for both CW and pulsed CO₂ laser cutting of mild steel. The upper and lower limits of these two pressure ranges when cutting thicker workpiece are lower than these when cutting the thinner workpiece. Hence, the pressure of the assist oxygen jet is reduced with increase in workpiece thickness at a constant laser power as shown in Fig. 2.28. The reduction in oxygen pressure is much lower than the reduction in cutting speed with increase in workpiece thickness [113].

The optimal cutting speed dramatically increases with increase in oxygen pressure at workpiece up to 2 bar and barely changes with oxygen pressure at workpiece increasing from 3.5 bar for cutting 8-mm-thick steel with both CW and pulsed lasers [113]. Small kerf width is achieved because both the thermal energy and mechanical energy provided by oxygen at this pressure range are sufficient and the melt flow is not macroscopically turbulent but periodic in the lower optimum pressure range and the controlled oxidation due to the reduction in macroscopic turbulence of the thinner molten layer by the increasing gas pressure in the higher optimum pressure range, respectively [113].

Gas Nozzle

Nozzle Types

- Subsonic nozzle

Nozzles which deliver the assist gas are generally subsonic nozzle with converging cross section as shown in Fig. 2.29. The characteristics of gas flow depend on the stagnation pressure, P_0 [121, 122]:

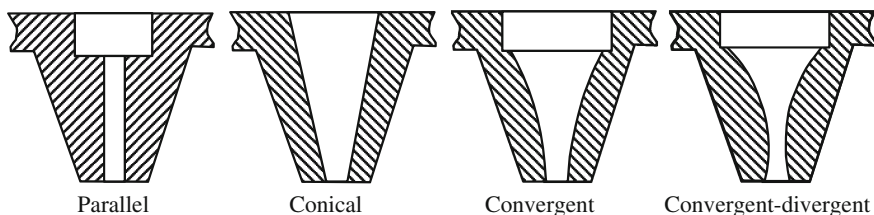


Fig. 2.29 Cross-sectional geometries of commonly used subsonic coaxial nozzle (reprinted from Fieret et al. [150] with permission. Copyright © SPIE)

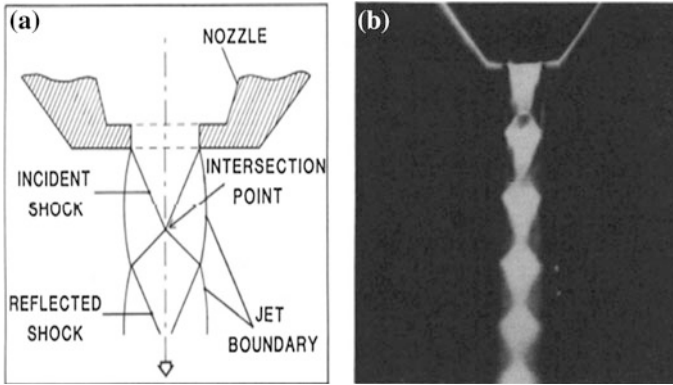
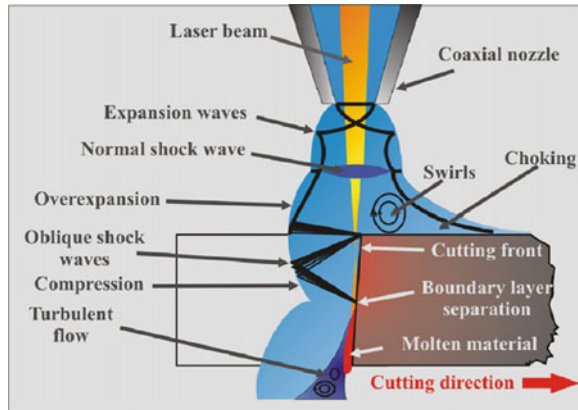


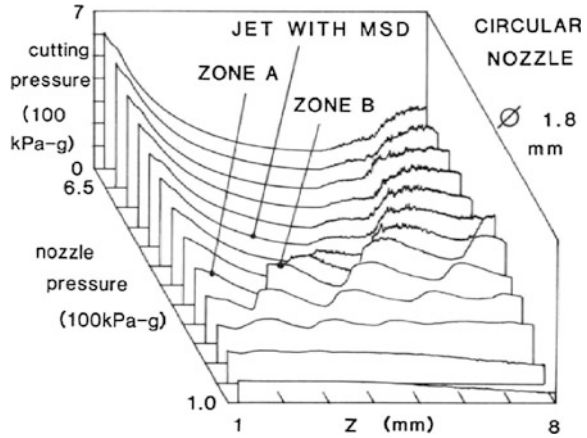
Fig. 2.30 **a** Illustration and **b** Schlieren image of Prandtl–Meyer wave (reprinted from Fieret et al. [150] with permission. Copyright © SPIE)

Fig. 2.31 Illustration of gas–melt interaction of supersonic gas flow with subsonic nozzle (reprinted from Riveiro et al. [95] with permission. Copyright © Elsevier)



1. $P_0 < 1.89 \text{ kg/cm}^2 (0.185 \text{ MPa})$: subsonic flow in which both gas velocity and flow increase with stagnation pressure;
2. $P_0 = 1.89 \text{ kg/cm}^2 (0.185 \text{ MPa})$: transonic flow in which gas velocity reaches the maximum value;
3. $P_0 > 1.89 \text{ kg/cm}^2 (0.185 \text{ MPa})$: supersonic flow in which gas velocity maintains the sonic velocity while gas flow increases with stagnation pressure. Prandtl–Meyer wave as shown in Fig. 2.30 is formed.
4. $P_0 > 5 \text{ kg/cm}^2 (0.49 \text{ MPa})$: supersonic flow in which strong Mach shock disk is formed (as shown in Fig. 2.31). The impingement of the oblique shock wave over the boundary layer produces a pressure gradient that may separate the boundary layer. The gas flow below the detachment point becomes turbulent with eddies and slipstreams that reduce the momentum transfer and the capability of the gas jet to remove the molten material and leads to the poor cut quality (increased dross attachment, heat-affected zone, and rough cut surface).

Fig. 2.32 Gas pressure at workpiece as a function of gas pressure in nozzle and distance from the nozzle exit, z for a circular nozzle (reprinted from Fieret et al. [151] with permission. Copyright © SPIE)



as shown in Fig. 2.17) [75, 121, 123]. The gradients of gas density that is produced by non-uniform jet flow results in a change of the refractive index in the gas field (acts like an optics), which leads to the secondary focusing or diverging of the laser beam. The result of interference can affect obviously the melting efficiency and change the mode of the laser beam, which causes poor cutting quality and reduces cutting speed [121].

The cutting pressure as a function of pressure in nozzle and distance between nozzle and workpiece surface (stand-off distance) for a conical subsonic nozzle is shown in Fig. 2.32. The gas pressure drops sharply in a very short distance from the exit of nozzle (with high nozzle pressure). Hence, the stand-off distance should be kept very small (smaller than the diameter of the nozzle), usually 0.3–1.3 mm for a subsonic nozzle in order to maintain the gas pressure [124].

- **Supersonic nozzle:**

Laval nozzle contains stable, convergent, throat, and divergent sections (Fig. 2.33a). The gas flow is supersonic at the Laval nozzle exit, and the free gas jet stays homogeneous with weak oblique shocks and parallel for a long distance (i.e., long supersonic length as shown in Fig. 2.33b) [122, 125]. Therefore, the toleration of stand-off distance with using Laval nozzle is greater compared with using subsonic nozzle [121].

The higher gas speed exits from Laval nozzle significantly improves the melt flow ejection, which leads to better cut quality in terms of small HAZ and less dross attachment.

Nozzle Integration

Gas nozzle can be integrated coaxially or off-axially with laser beam, or combined as shown in Fig. 2.34. The coaxial nozzles are generally used and are particularly

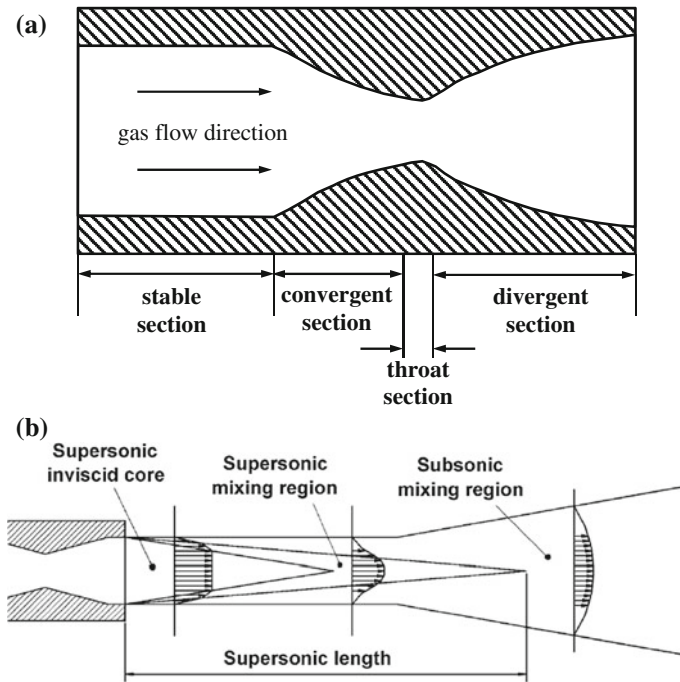


Fig. 2.33 **a** Typical cross section of a Laval nozzle and **b** supersonic length of gas jet by Laval nozzle (reprinted from Quintero et al. [125] with permission. Copyright © Elsevier)

suited for robotic systems performing two- and three-dimensional cutting, while the off-axis nozzle is useful for one-dimensional cutting [119].

The coaxial nozzle is discussed through this chapter. This section is focused on the special features of a single off-axis nozzle and an off-axial nozzle in tandem with the coaxial nozzle.

1. Off-axis nozzle

There are more parameters for adjusting an off-axis nozzle than a coaxial nozzle, including impinging angle between the axes of the laser beam and the gas jet, gap between the nozzle and the workpiece and distance between the impinging point of gas jet and the laser spot on workpiece surface (marked by X in Fig. 2.34b).

The off-axis is mounted after the laser beam in the cutting direction. Maximum cutting speed reaches the peak (50 % higher than that with the coaxial nozzle) with the impinging angle in the range of 35–40° without noticeable degradation in cut edge quality. This improvement is the result that the flow separation due to the shock wave/boundary layer interaction is alleviated [126].

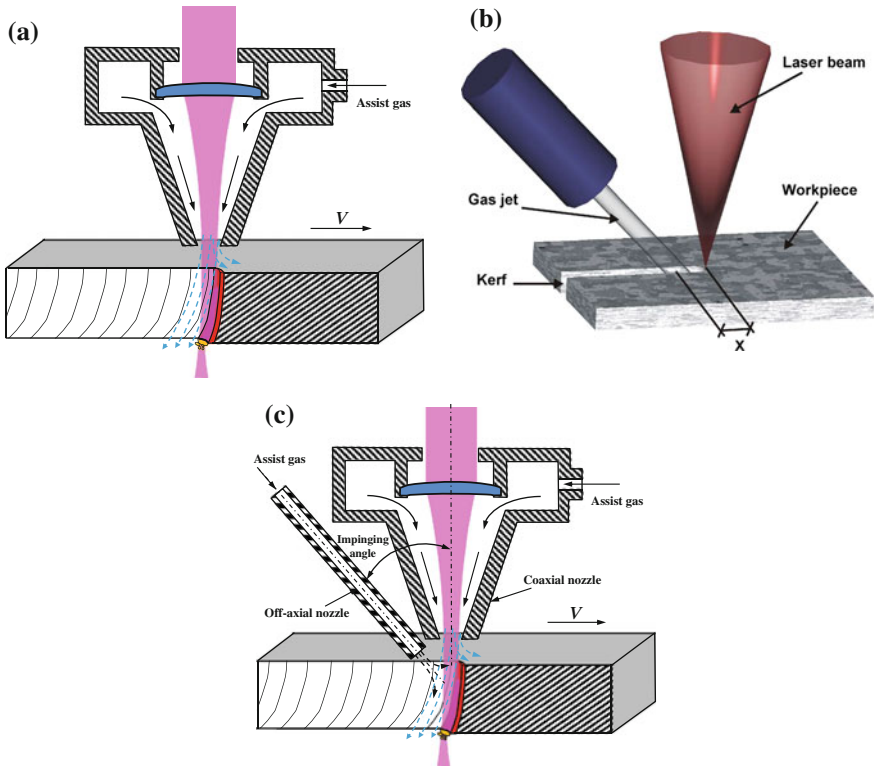


Fig. 2.34 Laser cutting with **a** coaxial, **b** off-axis (reprinted from Quintero et al. [125] with permission. Copyright © Elsevier), and **c** tandem nozzles

When the assist gas jet delivered by an off-axis nozzle impacts onto the cutting front close to 90° , the melt film can be confined near the cutting front in order to have a melt with large Weber numbers and to obtain dross-free cuts [46].

The gap between the nozzle and the workpiece should be smaller than the supersonic length. When a Laval nozzle is used, the impinging angle which determines the aerodynamic behavior of the gas flow inside the kerf should be adjusted in accordance with the Mach number of the nozzle to avoid the formation of a normal and detached shock wave. The distance between the impinging point of the gas jet and the laser beam should be adjusted in such way that a laminar flow is achieved along the whole depth of the cutting front in order to eliminate the formation of a recast layer on the cut edge in laser fusion cutting [123, 125].

2. Tandem nozzles

Use of an off-axis nozzle in tandem with the coaxial nozzle improves the cutting depth up to 20 %. Higher cutting depth is achieved with higher gas pressure, small nozzle-workpiece distance, and impinging angle [127].

Table 2.6 Summary of process parameters affecting cut surface quality (reprinted from Dubey and Yadava [20] with permission. Copyright © Elsevier)

Quality characteristics	Significant factors	Variation of factors to keep minimum value of quality characteristics
Heat-affected zone	Beam energy	Low
	Feed rate	High
	Pulse duration	High
	Pulse frequency	Moderate
	Gas pressure	More
	Workpiece thickness	Low
Taper	Beam energy	Low
	Feed rate	High
	Pulse frequency	Low
	Pulse duration	High
	Workpiece thickness	More
	Focus position	Above the workpiece surface
Surface roughness	Beam energy	Moderate
	Feed rate	Moderate
	Pulse frequency	Moderate
	Gas type	Inert
	Gas pressure	Moderate
Recast layer	Beam energy	High
	Pulse duration	Low
	Gas pressure	High
	Workpiece thickness	Low
	Focus position	Above the workpiece surface
Dross adherence	Gas type	Inert
	Gas pressure	High
	Beam energy	High
	Feed rate	High
	Pulse frequency	Low
Microcracks	Beam energy	High
	Pulse duration	Low
	Gas pressure	High
	Gas type	Inert

With a constant distance between coaxial and off-axis nozzles, material removal rate increases with decrease in impinging angle of the off-axis nozzle. Surface roughness becomes greater at small impinging angles which promotes turbulent flows due to the extended distance from the off-axial nozzle to the erosion-cutting front. The dross height is also affected by the impinging angle of off-axis angle [128].

Higher cutting speed with use of an off-axis nozzle in tandem with the coaxial nozzle in laser cutting is attributed to more effective momentum transfer. The formation of Cr_2O_3 in the melt during cutting stainless steel with oxygen jet is suppressed with the off-axis nozzle [128].

The application of an off-axis nozzle with coaxial cutting head is also reported to prevent ambient gas entrained in the gas flow and to eliminate the formation of vortex in the melt [73].

The effect of processing parameters on the cut quality is summarized in Table 2.6 for cutting with Nd:YAG laser [20].

2.3.3 Workpiece Aspects for Laser Beam Machining

2.3.3.1 Workpiece Thickness

There is a clear maximum material thickness for a particular laser–material combination for both laser fusion cutting and oxygen-assisted laser cutting, beyond which the cutting mechanism breaks down and cannot be reestablished at any speed because the relative increase in thermal losses from the cut zone as the cutting speed is decreased [64, 129]. The maximum thickness of workpiece is limited by the laser power and the shape of the focused laser beam as shown in Fig. 2.27 [4, 43]. It is recommended to increase nozzle diameter with increase in workpiece thickness in order to increase the kerf width [36, 68].

The maximum thickness of a workpiece can be cut at a given laser power decreases with decrease in waveguide attenuation as a fact that fraction of laser radiation transmitted through the kerf without absorbed by the cut front increases with decrease in waveguide attenuation [48].

There are some strategies developed to increase the maximum thickness that can be cut with the available laser power.

Dual Laser Beams

Laser beam is separated by a small distance trailing each other. The first beam partially penetrates the moving workpiece and forms a blind cylindrical keyhole. The second beam impinges the molten region produced by the first beam and further heats it vaporizing some material and superheating the remainder as shown in Fig. 2.35a. Improvement is achieved in terms of higher cutting speed and larger workpiece thickness as shown in Fig. 2.35b, which is attributed to improvement in beam absorption and modification of conduction characteristics.

Spinning Laser Beam

The laser beam is spun by a rotating window which is placed in the beam path at an angle to the beam axis, which causes the laser beam to form a spiral path when it travels across the workpiece. A linear relationship exists between the workpiece thickness and spin speed [130]. It has been demonstrated that mild steel and stainless steel with thickness up to 25 mm can be cut with spinning beam with 1.8 kW CO₂ laser.

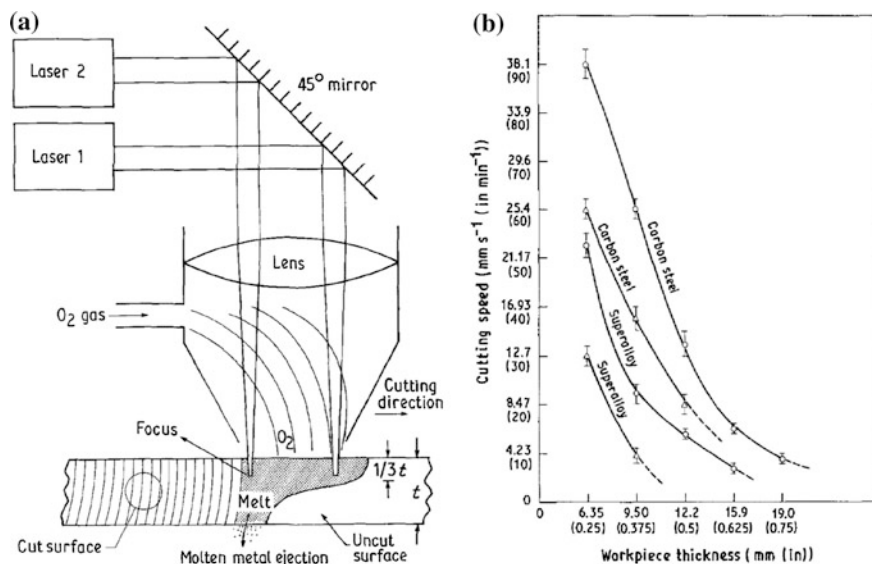


Fig. 2.35 **a** Schematic of cutting process by dual laser beams and **b** improvement of cutting speed compared with a single beam (reprinted from Molian [151] with permission. Copyright © Springer)

Laser-Assisted Oxygen Cutting (LASOX)

Reactive laser cutting of thicker steel plates requires higher-power laser, which not only increases capital cost but also often results in poor cut surface quality in terms of large heat-affected zone and severe striation. In order to generate extra heat, a process named LASOX was developed by O'Neill et al. at the University of Liverpool [131].

Differentiated from the conventional oxygen-assisted laser cutting, up to 80 % of total cutting energy is contributed by the exothermic heat generated from the combustion of iron. Laser beam is used to preheat the surface of workpiece to the ignition point ($\sim 1,237\text{ K}$). In order to completely use exothermic energy, the oxygen jet footprint is slightly smaller than the laser beam footprint as shown in Fig. 2.36. Thick mild steel plate of 50 mm can be cut at the incident laser power level of 1 kW.

2.3.3.2 Workpiece Materials

Ferrous Metals

The mild steel is easily cut with the oxygen as assist gas because of the contribution of exothermic heat. The oxide formed is easily removed from the kerf due

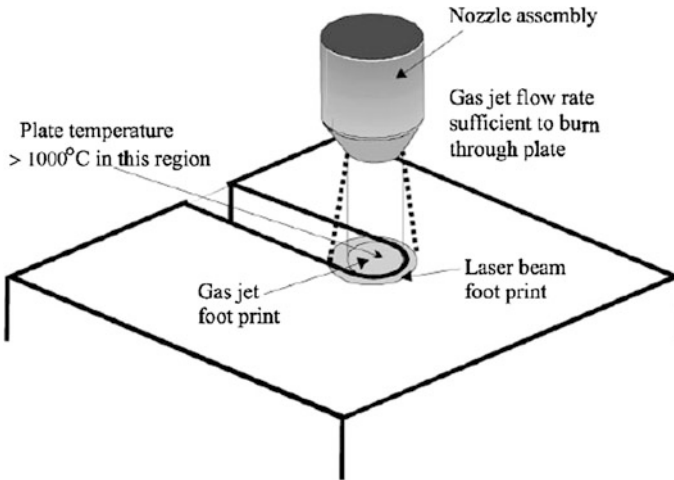


Fig. 2.36 Schematic illustration of laser beam/oxygen footprint configuration in LASOX process (reprinted from O'Neill and Gabzdy [131] with permission. Copyright © Elsevier)

to its low viscosity, and no significant dross is attached to the cut edge. Oxide layer is formed on the cut surface.

In reactive laser cutting of stainless steel, the oxide, Cr_2O_3 , formed with a high melting point of 2,435 °C that increases the viscosity and surface tension of the melt. The melt flow velocity is diminished, and the continuous oxidation of the melt cannot be achieved because oxygen cannot diffuse through the Cr_2O_3 layer [36].

The surface of stainless steel cut with oxygen as assist gas is not weldable, and the oxide layer must be removed to eliminate the porosity that occurs in welding [66]. Generally, high-pressure nitrogen is used as assist gas to produce oxide-free and dross-free cuts with laser focused at the bottom surface of workpiece [132].

Non-Ferrous Metals

It is difficult to cut aluminum alloys with laser because of their (1) high reflectivity, (2) high thermal conductivity, and (3) self-extinguishing oxidation reaction with using oxygen as assist gas which is attributed to the fact that aluminum oxide forms a seal on the cut front, which prevents oxygen from penetrating into the melt for further reaction before it is fractured. It is required to increase laser power in CW mode to initiate the cut in the first stage of the process; however, back-reflected beams entering into the laser cavity can damage the laser cavity, cavity optics, or beam delivery optics [95]. Therefore, pulsed laser with high peak power is beneficial for cutting aluminum alloys.

The cutting of aluminum alloy is strongly affected by the assist gas nature as shown in Table 2.7. Oxygen, nitrogen, and compressed air react with aluminum to

Table 2.7 Variation of cutting speed (V) surface roughness (Ra) and HAZ extension in descendent order with assist gas of aluminum alloy (reprinted from Riveiro et al. [94] with permission. Copyright © Elsevier)

	Cutting speed, V	Cut surface roughness, Ra	HAZ extension
(+)	Ar	O ₂	O ₂
↓	O ₂	N ₂	Air
(−)	Air	Air	N ₂
	N ₂	Ar	Ar

produce a large amount of oxides and/or nitrides. These oxides/nitrides attached to the lower cut edge as clinging dross increase the surface roughness and HAZ. Ar is more efficient assist gas to produce the best quality because of the increase in viscous friction with the melt as a result of its highest dynamic viscosity and density [94].

In cutting titanium alloys, a thin layer of hard and brittle oxide or nitride is formed on the cut surface when oxygen or nitrogen is used as assist gas. Thicker HAZ layers are produced due to the heat released from the nitriding and oxidation. Microcracks are formed on the cut surface as the results of tension forces on the laser cut surface and the brittleness of the titanium oxide and titanium nitride. The amount and dimensions of the microcracks can be reduced by increasing the cutting speed. The best corrosion resistance of the cut surface is achieved when cutting with Ar as assist gas [93].

The cut surface of titanium alloy is well protected by using He or Ar as assist gas. The maximum cutting speed is higher and cut edges are straight when cutting with Ar as assist gas compared with cutting with He as assist gas. The wavy cut edges and lower maximum cutting speed when cutting with He as assist gas are attributed to the lower cut front temperature as the result of high convective heat transfer coefficient of He as shown in Table 2.5. The low cut front temperature prevents melt front propagating ahead of the laser spot and limits the melt ejection from the cut zone at higher cutting speeds [97].

Ceramics

Alumina undergoes the following changes when it is subjected to heating [133]:

- Melting at $2,327\text{ K} \leq T < 3,500\text{ K}$,
- Dissociation to AlO (g), Al (l), Al(g), and Al₂O(g) at $3,250\text{ K} < T < 5,000\text{ K}$,
- Formation of aluminum vapor and atomic oxygen at $T > 5,000\text{ K}$.

Recoil pressure generated due to the dissociation process provoked expulsion of the melt film formed due to melting between 2,327 and 3,500 K [133]. Oxygen is normally used as the assist gas for cutting alumina to reduce the oxygen depletion and prevent alumina being discolored during laser fusion cutting [134].

One of the main problems in the laser cutting of ceramics is the formation of cracks induced by thermal stresses which are generated in the workpiece due to the local heating of the workpiece during laser irradiation, the brittle nature of ceramics, and the unique properties of ceramic materials (i.e., the high thermal expansion coefficient and low thermal conductivity) [123, 134].

The tendency of cracking when cutting 2-mm-thick alumina with CW CO₂ laser decreases with increase in laser power and decrease in feed rate, which lead to the reduction in temperature gradient [135]. An empirical equation is established for the boundary of cracking in terms of the operating conditions, the material properties, and thickness of the specimen as

$$P = 1.40 \times 10^{23} \rho_w \cdot g^{2.41} d^{2.41} r_L^{2.82} V \cdot c_w^{-1.41} \alpha_w^{1.41} \quad (2.29)$$

Crack-free cut can be achieved with pulsed laser with short pulse duration for cutting thin ceramic workpiece due to the lower heat input [135]. Cracking is inevitable when the pulse duration increases for cutting thick ceramic workpiece. Multiple passes with short pulse duration can be applied for cutting thick workpiece with low productivity [136–138].

Non-Homogenous Materials

Coated Metallic Materials

A thin layer of zinc and/or aluminum coated on both sides of sheet steels provides good corrosion resistance, but the higher light reflectivity and thermal conductivity, and the lower melting point of the coating layer than that of the substrate materials impose some difficulties and limitations on laser cutting [139].

Cutting speed is reduced when cutting coated steel because of the high reflectivity of the coating in CW laser cutting; however, the effect of coating on cutting speed with pulsed laser is not as significant as with CW laser [112].

Oxygen is quite effective as an assist gas for laser cutting the coated steel sheets as far as the cutting speeds are concerned because of the exothermic reaction between aluminum and oxygen. However, localized overheating and dross attachment are encountered with oxygen-assisted laser cutting. Dross- and oxidation-free cut can be achieved with high-pressure nitrogen [129].

Metal Laminates

Metal laminates are typically aluminum-based, with an aluminum sheet thickness in the order of 0.25 mm. Up to six aluminum sheets may be encountered in one laminate, which are filled up with a synthetic material, such as epoxy embedded glass or aramid fibers, or polypropylene. They can be applied in aeroplanes with advantages of enhanced fatigue resistance and weight reduction [140].

These materials can be cut with laser at the same speed as homogeneous aluminum alloys, with some damage on the synthetic layers and dross attachment

occurring. The damage depth of the synthetic layer is significantly reduced with increase in cutting speed up to 6 m/min. Primary interaction between laser beam and synthetic materials is not dominant in the damage extent of the synthetic layers. Heat input into the synthetic layers via the metal layers is most likely to be dominant [140].

Metal Matrix Composite Materials (MMCs)

Problems associated with laser cutting composites are the differences between matrix and reinforcements in laser absorption, melting point, latent heat of fusion, and specific heat capacity, which influence melting dynamics at the cut edges during the cutting process [141].

The material removal process in laser cutting SiC fiber-reinforced Al6061 composites (0/90 two-ply laminate) is melting of metal matrix and vaporization of SiC fiber [142].

There is a critical energy density for the cutting of the fiber and matrix, E_{crit}^f and E_{crit}^m , respectively, with $E_{\text{crit}}^f > E_{\text{crit}}^m$ in the case of SiC fiber-reinforced aluminum alloys. When the laser beam energy is higher than the critical value, E_{crit}^f , both the fiber and the matrix are removed simultaneously; however, when the laser beam energy ranges from E_{crit}^m to E_{crit}^f , only the matrix is removed. Consequently, at first, aluminum alloy matrix is melted and then evaporated and/or blown by the assist gas jet. Then, the bare SiC fiber is directly irradiated by the laser beam and then evaporated. Therefore, it is clear that the laser cutting phenomenon of metal matrix composites is strongly influenced by the laser cutting phenomena of the individual components [142].

In the particulate reinforced metal matrix composites, the specific heat capacity increases and the thermal conductivity decreases with increase in the volume fraction of the reinforcement particles, such as Al_2O_3 and B_4C , these lead to large kerf width. Al_2O_3 and B_4C particles remain in solid phases close to the cut edges. Al_2O_3 particles undergo high temperature reactions forming AlO at cut edges, whereas B_4C particles appear to be round and are present at the cut edges as solid particles [141].

Fiber-Reinforced Plastics (FRP)

Fiber-reinforced plastics, containing reinforcing fiber (glass fiber or carbon fiber etc.) and polymer matrix (GFRP and CFRP), offer high specific strength and are widely used for aerospace and sports industries. The alternative orientation of fiber and matrix creates the difficulties for conventional machining.

Laser beam machining is a suitable technology to cut FRP efficiently with minimum material waste, no tool wear, low overall distortion, or part damage. Nd:YAG and fiber lasers with wavelengths of 1.06 and 1.07 μm , respectively, are transparent to glass and therefore are not suitable for cutting glass fiber-reinforced plastics [143]. CO_2 laser is operated at a wavelength of 10.6 μm that can be

effectively absorbed by most organic materials [144], and therefore, is a suitable heat source for cutting FRP.

Because of the different properties of fiber and matrix, the energy required to vaporize the fibers is higher than that required for the matrix. This is more prominent for cutting carbon fiber-reinforced plastics because of the high disassociation temperature and high thermal conductivity of carbon fiber. Large amount of resin matrix is vaporized in the process. This causes delamination and matrix recession of the composite. The different removal rate between fibers and matrix produces the cut surface with fibers devoid of the matrix material [143].

For a given laser power, the maximum cutting speed achievable for CFRP is much lower than that for GFRP. It is visible on the cut surface, and the length of protruding fibers decreases with increase in cutting speed [145].

HAZ decreases with increase in cutting speed and assist gas pressure but independent of type of gas. Higher laser power leads to increase in the HAZ because of higher heat input [143].

Similar to that in cutting metallic workpiece, HAZ is reduced by using pulsed laser beam compared to using CW laser, due to the effective cooling between the pulses [143, 144].

2.4 Concluding Remarks

Laser beam is a unique machining source which can cut materials by photo-thermal processes, in which materials are separated by controlled fracture or locally removed by melt ejection, vaporization or ablation mechanisms.

In the melt and ejection process, a layer of melt (cut front) is formed and extends through the workpiece thickness, kerf is produced after the melt is removed by a pressurized gas jet. This process is able to cut large variety of materials, such as metals, ceramics, composites and glasses, etc.

The cut quality and maximum cutting speed are strongly affected by the (1) characteristics (wavelength, power, focusing and pulsing) of the laser beam, (2) the optical and thermophysical properties of the material, (3) thickness of workpiece and (4) type and pressure of assist gas.

The technology of laser cutting will continue to grow into the future as more powerful, flexible, efficient and compact systems become.

References

1. Meijer J (2004) Laser beam machining (LBM), state of the art and new opportunities. *J Mater Process Technol* 149:2–17
2. Tunna L, O'Neill W, Khan A, Sutcliffe C (2005) Analysis of laser micro drilled holes through aluminium for micro-manufacturing applications. *Opt Lasers Eng* 43:937–950

3. Li L (2000) The advances and characteristics of high-power diode laser materials processing. *Opt Lasers Eng* 34:231–253
4. Schuöcker D (1989) Laser cutting. *Mater Manuf Process* 4:311–330
5. Olsen FO, Alting L (1995) Pulsed laser materials processing, ND-YAG versus CO₂ lasers. *CIRP Ann—Manuf Technol* 44:141–145
6. Elijah Kannatey-Asibu J (2009) Principles of laser materials processing. Wiley, Hoboken
7. Yalukova O, Sárady I (2006) Investigation of interaction mechanisms in laser drilling of thermoplastic and thermoset polymers using different wavelengths. *Compos Sci Technol* 66:1289–1296
8. Bergström D, Powell J, Kaplan AFH (2007) A ray-tracing analysis of the absorption of light by smooth and rough metal surfaces. *J Appl Phys* 101:13504
9. Petring D, Abels P, Beyer E (1988) Absorption distribution on idealized cutting front geometries and its significance for laser beam cutting. *Proc SPIE* 1020:123–131
10. Kwon H, Yoh JJ (2012) Polarized reflectance of aluminum and nickel to 532, 355 and 266 nm Nd:YAG laser beams for varying surface finish. *Opt Laser Technol* 44:1823–1828
11. Mv Allmen (1976) Laser drilling velocity in metals. *J Appl Phys* 47:5460–5463
12. Chan CL, Mazumder J (1987) One-dimensional steady-state model for damage by vaporization and liquid expulsion due to laser-material interaction. *J Appl Phys* 62:4579–4586
13. Chang JJ, Warner BE (1996) Laser-plasma interaction during visible-laser ablation of metals. *Appl Phys Lett* 69:473–475
14. Tam SC, Williams R, Yang LJ, Jana S, Lim LEN, Lau MWS (1990) A review of the laser processing of aircraft components. *J Mater Process Technol* 23:177–194
15. Segall AE, Cai G, Akarapu R, Romasco A, Li BQ (2005) Fracture control of unsupported ceramics during laser machining using a simultaneous prescore. *J Laser Appl* 17:57–62
16. Tsai C-H, Chen H-W (2003) Laser cutting of thick ceramic substrates by controlled fracture technique. *J Mater Process Technol* 136:166–173
17. Kalyanasundaram D, Shrotriya P, Molian P (2010) Fracture mechanics—based analysis for hybrid laser/water jet (LWJ) machining of yttria-partially stabilized zirconia (Y-PSZ). *Int J Mach Tool Manuf* 50:97–105
18. Barnes C, Shrotriya P, Molian P (2007) Water-assisted laser thermal shock machining of alumina. *Int J Mach Tool Manuf* 47:1864–1874
19. Tsai CH, Liou CS (2003) Fracture mechanism of laser cutting with controlled fracture. *J Manuf Sci Eng, Trans ASME* 125:519–528
20. Dubey AK, Yadava V (2008) Experimental study of Nd:YAG laser beam machining—An overview. *J Mater Process Technol* 195:15–26
21. Mahrle A, Lütke M, Beyer E (2010) Fibre laser cutting: beam absorption characteristics and gas-free remote cutting. *Proc Inst Mech Eng C: J Mech Eng Sci* 224:1007–1018
22. Quintero F, Varas F, Pou J, Lusquiños F, Boutinguiza M, Soto R, Pérez-Amor M (2005) Theoretical analysis of material removal mechanisms in pulsed laser fusion cutting of ceramics. *J Phys D Appl Phys* 38:655–666
23. Olsen FO, Alting L (1989) Cutting front formation in laser cutting. *CIRP Ann—Manuf Technol* 38:215–218
24. Ivarson A, Powell J, Kamalu J, Magnusson C (1994) The oxidation dynamics of laser cutting of mild steel and the generation of striations on the cut edge. *J Mater Process Technol* 40:359–374
25. Arata Y, Maruo H, Miyamoto I, Takeuchi S (1979) Dynamic behaviour in laser cutting of mild steel. *Trans Jpn Weld Res Inst* 8:15–26
26. Chen K, Yao YL, Modi V (1999) Numerical simulation of oxidation effects in the laser cutting process. *Int J Adv Manuf Technol* 15:835–842
27. Kaplan AFH, Wangler O, Schuöcker D (1997) Laser cutting: fundamentals of the periodic striations and their on-line detection. *Lasers Eng* 6:103–126
28. Sobih M, Crouse PL, Li L (2007) Elimination of striation in laser cutting of mild steel. *J Phys D Appl Phys* 40:6908–6916

29. Kaplan AFH (1996) An analytical model of metal cutting with a laser beam. *J Appl Phys* 79:2198–2208
30. Fomin VM, A.G. Malikov, Orishich AM, Shulyat'ev VB (2011) Energy conditions of gas laser cutting of thick steel sheets. *J Appl Mech Tech Phys* 52:340–346
31. Mahrle A, Beyer E (2009) Theoretical aspects of fibre laser cutting. *J Phys D Appl Phys* 42:175507
32. Prusa JM, Venkitachalam G, Molian PA (1999) Estimation of heat conduction losses in laser cutting. *Int J Mach Tool Manuf* 39:431–458
33. Duan J, Man HC, Yue TM (2001) Modelling the laser fusion cutting process: I. Mathematical modelling of the cut kerf geometry for laser fusion cutting of thick metal. *J Phys D Appl Phys* 34:2127–2134
34. Schuöcker D (1986) Theoretical model of reactive gas-assisted laser cutting including dynamic effects. *Proc SPIE* 650:210–219
35. Ivarson A (1993) On the physics and chemical thermodynamics of laser cutting. PhD thesis, Lulea University of Technology, Sweden
36. Powell J (1998) *CO₂ Laser Cutting*. Springer, London
37. Ivarson A, Powell J, Magnusson C (1991) The role of oxidation in laser cutting stainless and mild steel. *J Laser Appl* 3:41–45
38. Hsu MJ, Molian PA (1994) Thermochemical modelling in CO₂ laser cutting of carbon steel. *J Mater Sci* 29:5607–5611
39. Powell J, Petring D, Kumar RV, Al-Mashikhi SO, Kaplan AFH, Voisey KT (2009) Laser-oxygen cutting of mild steel: the thermodynamics of the oxidation reaction. *J Phys D Appl Phys* 42:015504
40. Geiger M, Bergmann HW, Nuss R (1988) Laser cutting of steel sheets. *Proc SPIE* 1022:20–33
41. Chen S-L (1998) The effects of gas composition on the CO₂ laser cutting of mild steel. *J Mater Process Technol* 73:147–159
42. Powell J, Ivarson A, Magnusson C (1993) Laser cutting of steels: a physical and chemical analysis of the particles ejected during cutting. *J Laser Appl* 5:25–31
43. Poprawe R, König W (2001) Modeling, monitoring and control in high quality laser cutting. *CIRP Ann—Manuf Technol* 50:137–140
44. Yudin P, Kovalev O (2009) Visualization of events inside kerfs during laser cutting of fusible metal. *J Laser Appl* 21:39–45
45. Hirano K, Fabbro R (2011) Experimental investigation of hydrodynamics of melt layer during laser cutting of steel. *J Phys D Appl Phys* 44:105502
46. Riveiro A, Quintero F, Lusquiños F, Comesaña R, Pou J (2011) Study of melt flow dynamics and influence on quality for CO₂ laser fusion cutting. *J Phys D Appl Phys* 44:135501
47. Chen S-L (1997) In-process monitoring of the cutting front of CO₂ laser cutting with off-axis optical fibre. *Int J Adv Manuf Technol* 13:685–691
48. Schuöcker D, Abel W (1984) Material removal mechanism of laser cutting. *Proc SPIE* 455:88–95
49. Schuöcker D (1986) Dynamic phenomena in laser cutting and cut quality. *Appl Phys B* 40:9–14
50. Vicanek M, Simon G (1987) Momentum and heat transfer of an inert gas jet to the melt in laser cutting. *J Phys D Appl Phys* 20:1191–1196
51. Schulz W, Simon G, Urbassek HM, Decker I (1987) On laser fusion cutting of metals. *J Phys D Appl Phys* 20:481–488
52. Schulz W, Kostyrykin V, Nießen M, Michel J, Petring D, Kreutz EW, Poprawe R (1999) Dynamics of ripple formation and melt flow in laser beam cutting. *J Phys D Appl Phys* 32:1219–1228
53. Vicanek M, Simon G, Urbassek HM, Decker I (1987) Hydrodynamical instability of melt flow in laser cutting. *J Phys D Appl Phys* 20:140–145

54. Wandera C, Kujanpaa V (2010) Characterization of the melt removal rate in laser cutting of thick-section stainless steel. *J Laser Appl* 22:62–70
55. Hirano K, Fabbro R (2011) Experimental observation of hydrodynamics of melt layer and striation generation during laser cutting of steel. *Phys Procedia* 12(Part A):555–564
56. Powell J, Al-Mashikhi SO, Kaplan AFH, Voisey KT (2011) Fibre laser cutting of thin section mild steel: an explanation of the ‘striation free’ effect. *Opt Lasers Eng* 49:1069–1075
57. Schober A, Musiol J, Daub R, Feil J, Zaeh MF (2012) Experimental investigation of the cutting front angle during remote fusion cutting. *Phys Procedia* 39:204–212
58. Di Pietro P, Yao YL (1995) A numerical investigation into cutting front mobility in CO₂ laser cutting. *Int J Mach Tool Manuf* 35:673–688
59. Ermolaev GV, Kovalev OB, Orishich AM, Fomin VM (2006) Mathematical modelling of striation formation in oxygen laser cutting of mild steel. *J Phys D Appl Phys* 39:4236–4244
60. Li L, Sobih M, Crouse PL (2007) Striation-free laser cutting of mild steel sheets. *CIRP Ann—Manuf Technol* 56:193–196
61. Schuöcker D (1988) Heat conduction and mass transfer in laser cutting. *Proc SPIE* 952:592–599
62. Tsai MJ, Weng CI (1993) Linear stability analysis of molten flow in laser cutting. *J Phys D Appl Phys* 26:719–727
63. Schulz W, Simon G, Vicanek M, Decker I (1987) Influence of the oxidation process in laser gas cutting. *Proc SPIE* 801:331–336
64. Powell J, Ivarson A, Ohlsson L, Magnusson C (2000) Conductive losses experienced during CO₂ laser cutting. *High Temper Mater Process* 4:201–211
65. Onuseit V, Ahmed MA, Weber R, Graf T (2011) Space-resolved spectrometric measurements of the cutting front. *Phys Procedia* 12(Part A):584–590
66. Olsen FO (1994) Fundamental mechanisms of cutting front formation in laser cutting. *Proc SPIE* 2207:402–413
67. Chen K, Lawrence Yao Y (1999) Striation formation and melt removal in the laser cutting process. *J Manuf Process* 1:43–53
68. Heidenreich B, Jüptner W, Sepold G (1996) Fundamental investigations of the burn-out phenomenon of laser cut edges. *Lasers Eng* 5:1–10
69. Wee LM, Li L (2005) An analytical model for striation formation in laser cutting. *Appl Surf Sci* 247:277–284
70. Duan J, Man HC, Yue TM (2001) Modelling the laser fusion cutting process: III. Effects of various process parameters on cut kerf quality. *J Phys D Appl Phys* 34:2143–2150
71. Chen K, Lawrence Yao Y, Modi V (2001) Gas dynamic effects on laser cut quality. *J Manuf Process* 3:38–49
72. Ermolaev GV, Kovalev OB (2009) Simulation of surface profile formation in oxygen laser cutting of mild steel due to combustion cycles. *J Phys D Appl Phys* 42:185506
73. Kovalev OB, Yudin PV, Zaitsev AV (2008) Formation of a vortex flow at the laser cutting of sheet metal with low pressure of assisting gas. *J Phys D Appl Phys* 41:155112
74. Farooq K, Kar A (1998) Removal of laser-melted material with an assist gas. *J Appl Phys* 83:7467–7473
75. Kovalev OB, Yudin PV, Zaitsev AV (2009) Modeling of flow separation of assist gas as applied to laser cutting of thick sheet metal. *Appl Math Model* 33:3730–3745
76. Karatas C, Keles O, Uslan I, Usta Y (2006) Laser cutting of steel sheets: influence of workpiece thickness and beam waist position on kerf size and stria formation. *J Mater Process Technol* 172:22–29
77. Kaebernick H, Bicleanu D, Brandt M (1999) Theoretical and experimental investigation of pulsed laser cutting. *CIRP Ann—Manuf Technol* 48:163–166
78. Decker I, Ruge J, Atzert U (1984) Physical models and technological aspects of laser gas cutting. *Proc SPIE* 455:81–87
79. Sobih M, Crouse PL, Li L (2008) Striation-free fibre laser cutting of mild steel sheets. *Appl Phys A* 90:171–174

80. Ledenev VI, Karasev VA, Yakunin VP (1999) On cyclical mechanism of kerf formation under gas assisted laser cutting of metals. *Proc SPIE* 3688:157–162
81. Di Pietro P, Yao YL (1995) A new technique to characterize and predict laser cut striations. *Int J Mach Tool Manuf* 35:993–1002
82. Schuöcker D, Aichinger J, Majer R (2012) Dynamic phenomena in laser cutting and process performance. *Phys Procedia* 39:179–185
83. Makashev NK, Asmolov ES, Blinkov VV, Boris AY, Burmistrov AV, Buzykin V, Makarov VA (1994) Gas-hydro-dynamics of CW laser cutting of metals in inert gas. *Proc SPIE* 2257:2–9
84. King TG, Powell J (1986) Laser-cut mild steel—factors affecting edge quality. *Wear* 109:135–144
85. Kaebernick H, Jeromin A, Mathew P (1998) Adaptive control for laser cutting using striation frequency analysis. *CIRP Ann—Manuf Technol* 47:137–140
86. Yan Y, Li L, Sezer K, Whitehead D, Ji L, Bao Y, Jiang Y (2012) Nano-second pulsed DPSS Nd: YAG laser striation-free cutting of alumina sheets. *Int J Mach Tool Manuf* 53:15–26
87. Dahotre NB, Harimkar SP (2008) *Laser Fabrication and Machining of Materials*. Springer, New York
88. Arata Y, Maruo H, Miyamoto I, Takeuchi S (1981) Quality in laser-gas-cutting stainless steel and its improvement. *Trans Jpn Weld Res Inst* 10:129–139
89. Nielsen SE (1997) Developments in laser beam cutting of thick materials. *Industrial Laser Review* 12: 11–13
90. Chen S-L (1999) The effects of high-pressure assistant-gas flow on high-power CO₂ laser cutting. *J Mater Process Technol* 88:57–66
91. O'Neill W, Steen WW (1995) A three-dimensional analysis of gas entrainment operating during the laser-cutting process. *J Phys D Appl Phys* 28:12–18
92. Sheng PS, Joshi VS (1995) Analysis of heat-affected zone formation for laser cutting of stainless steel. *J Mater Process Technol* 53:879–892
93. Shanjin L, Yang W (2006) An investigation of pulsed laser cutting of titanium alloy sheet. *Opt Lasers Eng* 44:1067–1077
94. Riveiro A, Quintero F, Lusquiños F, Comesaña R, Pou J (2010) Influence of assist gas nature on the surfaces obtained by laser cutting of Al–Cu alloys. *Surf Coat Technol* 205:1878–1885
95. Riveiro A, Quintero F, Lusquiños F, Comesaña R, Pou J (2010) Parametric investigation of CO₂ laser cutting of 2024–T3 alloy. *J Mater Process Technol* 210:1138–1152
96. Quintero F, Pou J, Lusquiños F, Boutinguiza M, Soto R, Pérez-Amor M (2004) Quantitative evaluation of the quality of the cuts performed on mullite-alumina by Nd:YAG laser. *Opt Lasers Eng* 42:327–340
97. Rao BT, Kaul R, Tiwari P, Nath AK (2005) Inert gas cutting of titanium sheet with pulsed mode CO₂ laser. *Opt Lasers Eng* 43:1330–1348
98. Scintilla LD, Tricarico L, Wetzig A, Mahrle A, Beyer E (2011) Primary losses in disk and CO₂ laser beam inert gas fusion cutting. *J Mater Process Technol* 211:2050–2061
99. Powell J, Ivarson A, Kamalu J, Broden G, Magnusson C (1993) Role of oxygen purity in laser cutting of mild steel. *Proc SPIE* 1990:433–442
100. Belic I, Stanic J (1987) A method to determine the parameters of laser iron and steel cutting. *Opt Laser Technol* 19:309–311
101. Belić I (1989) A method to determine the parameters of laser cutting. *Opt Laser Technol* 21:277–278
102. Chryssolouris G (1991) *Laser Machining, Theory and Practice*. Springer, New York
103. Lepore M, Dell'Erba M, Esposito C, Daurelio G, Cingolani A (1983) An investigation of the laser cutting process with the aid of a plane polarized CO₂ laser beam. *Opt Lasers Eng* 4:241–251
104. Muys P, Youn M (2008) Mathematical Modeling of Laser Sublimation Cutting. *Laser Phys* 18:495–499

105. Niziev V, Nesterov A (1999) Influence of beam polarization on laser cutting efficiency. *J Phys D Appl Phys* 32:1455–1461
106. Scintilla LD, Tricarico L, Mahrle A, Wetzig A, Beyer E (2012) A comparative study of cut front profiles and absorptivity behavior for disk and CO₂ laser beam inert gas fusion cutting. *J Laser Appl* 24:052006
107. Poprawe R, Schulz W, Schmitt R (2010) Hydrodynamics of material removal by melt expulsion: perspectives of laser cutting and drilling. *Phys Procedia* 5(Part A):1–18
108. Olsen FO, Hansen KS, Nielsen JS (2009) Multibeam fiber laser cutting. *J Laser Appl* 21:133–138
109. Petring D, Molitor T, Schneider F, Wolf N (2012) Diagnostics, modeling and simulation: three keys towards mastering the cutting process with fiber, disk and diode lasers. *Phys Procedia* 39:186–196
110. Wandera C, Kujanpää V, Salminen A (2011) Laser power requirement for cutting thick-section steel and effects of processing parameters on mild steel cut quality. *Proc Inst Mech Eng B J Eng Manuf* 225:651–661
111. Sparkes M, Gross M, Celotto S, Zhang T, O'Neill W (2008) Practical and theoretical investigations into inert gas cutting of 304 stainless steel using a high brightness fiber laser. *J Laser Appl* 20:59–67
112. Grevey DF, Desplats H (1994) Comparison of the performance obtained with a YAG laser cutting according to the source operation mode. *J Mater Process Technol* 42:341–348
113. Ivarson A, Powell J, Magnusson C (1996) The role of oxygen pressure in laser cutting mild steels. *J Laser Appl* 8:191–196
114. Thawari G, Sundar JKS, Sundararajan G, Joshi SV (2005) Influence of process parameters during pulsed Nd:YAG laser cutting of nickel-base superalloys. *J Mater Process Technol* 170:229–239
115. Bicleanu D, Brandt M, Kaebernick H (1996) An analytical model for pulsed laser cutting of metals. In: *Proceedings 15th international congress on applications of lasers and electro-optics*, 68–77
116. Lee CS, Gael A, Osada H (1985) Parametric studies of pulsed-laser cutting of thin metal plates. *J Appl Phys* 58:1339–1343
117. Pfeifer R, Herzog D, Hustedt M, Barcikowski S (2010) Pulsed Nd:YAG laser cutting of NiTi shape memory alloys—Influence of process parameters. *J Mater Process Technol* 210:1918–1925
118. Powell J, Tan WK, MacLennan P, Rudd D, Wykes C, Engstrom H (2000) Laser cutting stainless steel with dual focus lenses. *J Laser Appl* 12:224–231
119. Rocca AVL, Borsati L, Cantello M (1994) Nozzle design to control fluid-dynamics effects in laser cutting. *Proc SPIE* 2207:354–368
120. Powell J, Frass K, Menzies IA (1987) 2.5 kW Laser cutting of steels; Factors affecting cut quality in sections up to 20 mm. *Proc SPIE* 801:278–282
121. Man HC, Duan J, Yue TM (1997) Design and characteristic analysis of supersonic nozzles for high gas pressure laser cutting. *J Mater Process Technol* 63:217–222
122. Leidinger D, Penz A, Schuöcker D (1995) Improved manufacturing processes with high power lasers. *Infrared Phys Technol* 36:251–266
123. Quintero F, Pou J, Lusquiños F, Boutinguiza M, Soto R, Pérez-Amor M (2003) Comparative study of the influence of the gas injection system on the Nd:yttrium-aluminum-garnet laser cutting of advanced oxide ceramics. *Rev Sci Instrum* 74:4199–4205
124. Na SJ, Yang YS, Koo HM, Kim TK (1989) Effect of shielding gas pressure in laser cutting of sheet metals. *Trans ASME J Eng Mater Technol* 111:314–318
125. Quintero F, Pou J, Fernández JL, Doval AF, Lusquiños F, Boutinguiza M, Soto R, Pérez-Amor M (2006) Optimization of an off-axis nozzle for assist gas injection in laser fusion cutting. *Opt Lasers Eng* 44:1158–1171
126. Brandt AD, Settles GS (1997) Effect of nozzle orientation on gas dynamics of inert gas laser cutting of mild steel. *J Laser Appl* 9:269–277
127. Chryssolouris G, Choi WC (1989) Gas jet effects on laser cutting. *Proc SPIE* 1042:86–96

128. Hsu MJ, Molian PA (1995) Off-axial, gas-jet-assisted, laser cutting of 6.35-mm thick stainless steel. *Trans ASME J Eng Ind* 117:272–276
129. Prasad GVS, Siores E, Wong WCK (1998) Laser cutting of metallic coated sheet steels. *J Mater Process Technol* 74:234–242
130. Arai T, Riches S (1997) Thick plate cutting with spining laser beam. In: *Proceedings 16th international congress on applications of lasers and electro-optics*, 19–26
131. O'Neill W, Gabzdy JT (2000) New developments in laser-assisted oxygen cutting. *Opt Lasers Eng* 34:355–367
132. Ghany KA, Newishy M (2005) Cutting of 1.2 mm thick austenitic stainless steel sheet using pulsed and CW Nd:YAG laser. *J Mater Process Technol* 168:438–447
133. Samant AN, Dahotre NB (2009) Laser machining of structural ceramics—A review. *J Europ Ceram Soc* 29:969–993
134. Yan Y, Li L, Sezer K, Whitehead D, Ji L, Bao Y, Jiang Y (2011) Experimental and theoretical investigation of fibre laser crack-free cutting of thick-section alumina. *Int J Mach Tool Manuf* 51:859–870
135. Lu G, Siores E, Wang B (1999) An empirical equation for crack formation in the laser cutting of ceramic plates. *J Mater Process Technol* 88:154–158
136. Black I, Chua KL (1997) Laser cutting of thick ceramic tile. *Opt Laser Technol* 29:193–205
137. Black I, Livingstone SAJ, Chua KL (1998) A laser beam machining (LBM) database for the cutting of ceramic tile. *J Mater Process Technol* 84:47–55
138. Lei H, Lijun L (1999) A study of laser cutting engineering ceramics. *Opt Laser Technol* 31:531–538
139. Wang J, Wong WCK (1999) CO₂ laser cutting of metallic coated sheet steels. *J Mater Process Technol* 95:164–168
140. De Graaf RF, Meijer J (2000) Laser cutting of metal laminates: analysis and experimental validation. *J Mater Process Technol* 103:23–28
141. Yilbas BS, Khan S, Raza K, Keles O, Ubeyli M, Demir T, Karakas MS (2010) Laser cutting of 7,050 Al alloy reinforced with Al₂O₃ and B₄C composites. *Int J Adv Manuf Technol* 50:185–193
142. Kagawa Y, Utsunomiya S, Kogo Y (1989) Laser cutting of CVD-SiC fibre/A6061 composite. *J Mater Sci Lett* 8:681–683
143. Cenna AA, Mathew P (1997) Evaluation of cut quality of fibre-reinforced plastics—A review. *Int J Mach Tool Manuf* 37:723–736
144. Mello MD (1986) Laser cutting of non-metallic composites. *Proc SPIE* 668:288–290
145. Caprino G, Tagliaferri V (1988) Maximum cutting speed in laser cutting of fiber reinforced plastics. *Int J Mach Tool Manuf* 28:389–398
146. Ready JF (1997) *Industrial Applications of Lasers*. Academic Press, San Diego
147. Migliore L (1996) Laser-material interactions. In: Migliore L (ed) *Laser Materials Processing*. Marcel Dekker, Inc., New York
148. Rofin (2004) Introduction to industrial laser materials processing. http://www.obrusn.torun.pl/htm0/prod_images/rofin/Laserbook.pdf. Accessed 23 August 2012
149. Olsen FO (2011) Laser cutting from CO₂ laser to disk or fiber laser—possibilities and challenges. In: *Proceedings 30th international congress on applications of lasers and electro-optics*, Paper #101
150. Fieret J, Terry MJ, Ward BA (1986) Aerodynamic interactions during laser cutting. *Proc SPIE* 668:53–62
151. Fieret J, Terry MJ, Ward BA (1987) Overview of flow dynamics in gas-assisted laser cutting. *Proc SPIE* 801:243–250
152. Molian PA (1993) Dual-beam CO₂ laser cutting of thick metallic materials. *J Mater Sci* 28:1738–1748
153. Toyserkani E, Khajepour A, Corbin S (2005) *Laser Cladding*. CRC Press LLC, Boca Raton
154. Nath AK (2013) High power lasers in material processing applications: an overview of recent development. In: Majumdar JD, Manna I (eds) *Laser-assisted fabrication of materials*. Springer-Verlag, Berlin

155. Steen WM, Mazumder J (2010) *Laser Material Processing*. Springer, London
156. Powell J, Frass K, Menzies IA, Fuhr H (1988) CO₂ laser cutting of non-ferrous metals. *Proc SPIE* 1020:156–163
157. Riveiro A, Quintero F, Lusquiños F, Comesaña R, del Val J, Pou J (2011) The role of the assist gas nature in laser cutting of aluminum alloys. *Phys Procedia* 12(Part A): 548–554

Nontraditional Machining Processes

Research Advances

Davim, J.P. (Ed.)

2013, X, 232 p. 156 illus., Hardcover

ISBN: 978-1-4471-5178-4